Journal for ImmunoTherapy of Cancer

Single-cell transcriptomics reveals a low CD8$^+$ T cell infiltrating state mediated by fibroblasts in recurrent renal cell carcinoma

Yu-Lu Peng ,[1,2] Long-Bin Xiong,[1,2] Zhao-Hui Zhou,[1,2] Kang Ning,[1,2] Zhen Li,[1,2] Ze-Shen Wu,[3] Min-Hua Deng,[1,2] Wen-Su Wei,[1,2] Ning Wang,[1,2] Xiang-Peng Zou,[1,2] Zhi-Song He,[4] Ji-Wei Huang,[5] Jun-Hang Luo ,[6] Jian-Ye Liu,[7] Nan Jia,[8] Yun Cao,[2,9] Hui Han,[1,2] Sheng-Jie Guo,[1,2] Pei Dong,[1,2] Chun-Ping Yu,[1,2] Fang-Jian Zhou,[1,2] Zhi-Ling Zhang[1,2]

To cite: Peng Y-L, Xiong L-B, Zhou Z-H, *et al*. Single-cell transcriptomics reveals a low CD8$^+$ T cell infiltrating state mediated by fibroblasts in recurrent renal cell carcinoma. *Journal for ImmunoTherapy of Cancer* 2022;**10**:e004206. doi:10.1136/jitc-2021-004206

► Additional supplemental material is published online only. To view, please visit the journal online (http://dx.doi.org/10.1136/jitc-2021-004206).

Y-LP, L-BX and Z-HZ contributed equally.

Accepted 03 January 2022

For numbered affiliations see end of article.

Correspondence to
Professor Zhi-Ling Zhang; zhangzhl@sysucc.org.cn

Professor Fang-Jian Zhou; zhoufj@sysucc.org.cn

Dr Chun-Ping Yu; yuchp@sysucc.org.cn

ABSTRACT

Purpose Recurrent renal cell carcinoma(reRCC) is associated with poor prognosis and the underlying mechanism is not yet clear. A comprehensive understanding of tumor microenvironment (TME) of reRCC may aid in designing effective anticancer therapies, including immunotherapies. Single-cell transcriptomics holds great promise for investigating the TME, however, this technique has not been used in reRCC. Here, we aimed to explore the difference in the TME and gene expression pattern between primary RCC (pRCC) and reRCC at single-cell level.

Experimental design We performed single-cell RNA sequencing analyses of 32,073 cells from 2 pRCC, 2 reRCC, and 3 adjacent normal kidney samples. 41 pairs of pRCC and reRCC samples were collected as a validation cohort to assess differences observed in single-cell sequencing. The prognostic significance of related cells and markers were studied in 47 RCC patients underwent immunotherapy. The function of related cells and markers were validated via in vitro and in vivo experiments.

Results reRCC had reduced CD8$^+$ T cells but increased cancer-associated fibroblasts (CAFs) infiltration compared with pRCC. Reduced CD8$^+$ T cells and increased CAFs infiltration were significantly associated with a worse response from immunotherapy. Remarkably, CAFs showed substantial expression of LGALS1 (Gal1). In vitro, CAFs could induce CD8$^+$ T cells apoptosis via Gal1. In vivo, knockdown of Gal1 in CAFs suppressed tumor growth, increased CD8$^+$ T cells infiltration, reduced the proportion of apoptotic CD8$^+$ T cells and enhanced the efficacy of immunotherapy.

Conclusions We delineated the heterogeneity of reRCC and highlighted an innovative mechanism that CAFs acted as a suppressor of CD8$^+$ T cells via Gal1. Targeting Gal1 combined with anti-PD1 showed promising efficacy in treating RCC.

INTRODUCTION

Renal cell carcinoma (RCC) is one of the most common malignant tumors of the urinary system, with an annual worldwide increase of ~2% in incidence during the last two decades.[1] So far, surgery remains the most effective therapy for clinically localized RCC.[2] However, about 20% of patients with RCC develop recurrence after surgical excision.[3–6] Recurrent RCC (reRCC) represents a major clinical challenge and patients who experienced failure from local therapy often have poor prognosis.[5] Although immune checkpoint blockade therapy and combination regimens have increased the survival of RCC patients, the prognosis of patients with advanced RCC, including reRCC, remains poor.[7–9] A thorough investigation of reRCC could enhance our understanding on the mechanisms of tumor development and progression, and more importantly, facilitate the discovery of more effective therapeutic regimens for RCC.

The tumor microenvironment (TME) is a complex ecosystem composed of several cell types, including immune cells, cancer-associated fibroblasts (CAFs), endothelial cells, and extracellular matrix (ECM), which plays a critical role in cancer progression.[10] Among the immune cells infiltrating the TME, T cell, especially CD8$^+$ T cell, is a key antitumor immune component. The success of immunotherapy depends on the activation of a potent cytotoxic T cell response.[11] CAFs are the most abundant stromal cells in the TME and critically contribute to cancer progression.[12] Numerous studies have shown that CAFs can promote cancer via multiple processes including, but not limited to, cancer stem-cell renewal,[13] chemoresistance,[14] and immune-cell evasion.[14 15] Furthermore, there have been series of studies suggesting

that CAFs can blunt immunotherapy efficacy, and thus, CAFs have been regarded as an emerging target of anticancer immunotherapy.[14 16] Although various mechanisms related to the immunosuppressive features of CAFs have been reported, the mechanism of immunotherapy resistance mediated by CAFs is complicated and deserves further investigation.

Tumors secrete various growth factors and cytokines to shape an immunosuppressive TME. Galectin-1 (Gal1), a well-known immunosuppressor, can induce apoptosis of activated T cells and suppress T cell-mediated cytotoxic immune responses.[17–19] It is reported that Gal1 was highly expressed in multiple cell types including CAFs and could be secreted into the surrounding milieu of tumor.[20–23] Gal1 secreted by CAFs could promote epithelial-mesenchymal transformation in gastric cancer[24] and targeting Gal1 in CAFs has been shown to be able to inhibit oral squamous cell carcinoma metastasis.[25] However, the role of CAFs-derived Gal1 in the tumor immune microenvironment remains undetermined.

Single-cell RNA sequencing (scRNA-seq) is a promising method to investigate the cellular components and their interactions in the TME with high resolution.[26 27] ScRNA-seq has been used to distinguish the precise cellular identities and compositions of human kidney tumors.[28] Kim *et al*[29] unraveled the utility and validity of single-cell sequencing for the design of personalized therapeutic strategies in patients with metastatic RCC. A series of recent studies have examined the characteristics of TME in RCC patients using single-cell sequencing,[30–33] however, all these studies have focused on primary or metastatic tumors. Moreover, previous studies comparing primary versus recurrent tumors suggested that secondary tumors can be completely different in TME and gene expression from the primary tumor.[26 34] Thus, a comprehensive depiction of the differences between primary RCC (pRCC) and reRCC at the single-cell resolution level remains in urgent need.

In this study, we used scRNA-seq to profile single cells from pRCC and reRCC. Clinical paired pRCC and reRCC tumor samples were used to validate the differences observed in single-cell sequencing via immunohistochemistry (IHC). The prognostic significance of related cells and markers were studied in RCC patients who received immunotherapy. The function of related cells and markers were assessed via in vivo experiment. This study could improve our understanding on the mechanisms associated with tumor development and recurrence in RCC at the single-cell level.

METHODS

This study was performed in accordance with the ethical standards of the Helsinki Declaration and the ethical guidelines for Medical and Health Research Involving Human Subjects. Written informed consent was obtained for each of the participant patients. All cases were deidentified and personal identifiable details were removed from their case descriptions to ensure anonymity. This study was approved and reviewed by the Ethics Review Board of Sun Yat-sen University Cancer Center (SYSUCC). Mouse experiments were performed in a specific pathogen-free environment at the animal laboratory of the SYSUCC according to institutional guidelines, and all animal experimental protocols were approved and reviewed by the Ethics Review Committee for Animal Experimentation of SYSUCC. All experiments were performed in accordance with the guidelines and regulations indicated by these committees.

Experimental design

We performed single-cell sequencing on tumor tissue of two patients, who had local reRCC after nephrectomy and had recurrent tumor resection at SYSUCC. In parallel, the scRNA-seq data of 2 pRCC and 3 adjacent normal kidney samples described by Young *et al*[28] which is the first study characterizing treatment naïve pRCC using scRNA-seq, were downloaded for integrative analyses (figure 1A, online supplemental table S1). The validation cohort containing 41 pairs of pRCC and reRCC samples were retrospectively collected to assess differences observed in single-cell sequencing via IHC. The prognostic significance of related cells and markers were studied in SYSUCC immunotherapy cohort including 47 advanced RCC patients who underwent anti-PD1 immunotherapy and in the The Cancer Genome Atlas (TCGA) cohort. The function of related cells and markers were validated via in vitro and in vivo experiments. For further details regarding the materials and methods, please refer to the online supplemental methods.

RESULTS

Patient cohorts

The study was designed and conducted as illustrated in figure 1A,B. reRCC tissues were obtained from two patients diagnosed with local relapsed clear cell RCC in SYSUCC. The pathological type was renal clear cell carcinoma. Moreover, we recruited 41 patients with paired pRCC and reRCC samples to perform IHC to confirm differences found in the scRNA-seq. In this study, recurrent cancer within the renal fossa qualify as reRCC after partial nephrectomy or radical nephrectomy. In these 41 patients, 36 patients (87.8%) had a reRCC within 5 years. According to pathological typing, 34 patients (82.9%) had clear cell carcinoma, and 7 (17.1%) a papillary RCC. All patients had no change in the pathological type when experience tumor recurrence. Forty-seven RCC patients who received immunotherapy in our center were included in the SYSUCC immunotherapy cohort. We defined progression-free survival (PFS) as the time from immunotherapy initiation to disease progression or death from any cause. The available clinical features of the SYSUCC immunotherapy cohort are summarized in online supplemental table S2. scRNA-seq profiling of the tumor ecosystem in pRCC and reRCC.

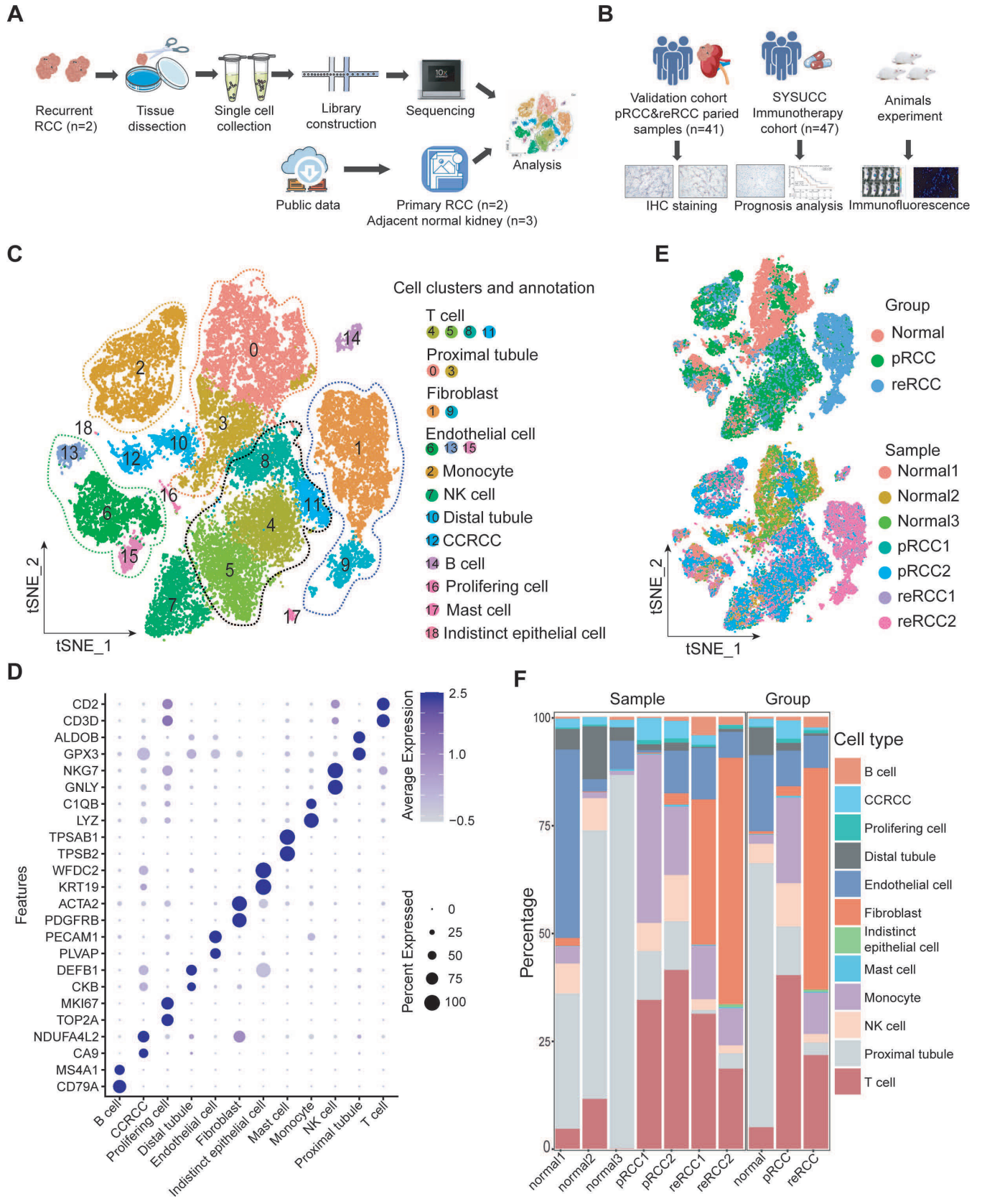

Figure 1 scRNA-seq profiling of the tumor ecosystem in adjacent normal kidneys, pRCC and reRCC. (A, B) Schematic representation of the experimental design. (C) The t-SNE plot, showing the annotation and color codes for cell types in the RCC ecosystem. (D) Dotplot showing the expression of marker genes in the indicated cell types. (E) The t-SNE plot, showing cell origins by color, groups origin and patients origin. (F) Histogram showing the percentage of cell types in samples and groups. IHC, immunohistochemistry; pRCC, primary renal cell carcinoma; RCC, renal cell carcinoma; reRCC, recurrent renal cell carcinoma; SYSUCC, Sun Yat-sen University Cancer Center; t-SNE: T-distributed stochastic neighbor embedding.

After quality control and removal of the batch effect between samples, 32,073 single cells were clustered into 19 major clusters using the T-distributed stochastic neighbor embedding (t-SNE) method. Cluster-specific genes were used to annotate cell types with classic markers described in previous studies.[26 31 35–37] We identified four types of epithelial cells in five clusters, including proximal tubule cells (ALDOB$^+$ and GPX3$^+$), cancer cells (CA9$^+$ and NDUFA4L2$^+$), distal tubule cells (DEFB1$^+$ and CKB$^+$), and indistinct epithelial cells (KRT19$^+$ and WFDC2$^+$); 5 types of immune cells in eight clusters, including T cells (CD3D$^+$ and CD2$^+$), NK cell (NKG7$^+$ and GNLY$^+$), monocytes (LYZ$^+$ and C1QB$^+$), B cells (CD79A$^+$ and MS4A1$^+$), and mast cells (TPSAB1$^+$ and TPSB2$^+$); fibroblasts (PDGFRB$^+$ and ACTA2$^+$); vascular endothelial (PECAM1$^+$ and PLVAP$^+$) and profiling cells (TOP2A$^+$ and MKI67$^+$) (figure 1C,D, online supplemental table S4). In adjacent normal kidney samples, proximal tubule cells and distal tubule cells were the most abundant cell types, with a low abundance of immune cell infiltration. In tumor samples, T cells and monocytes were the main infiltrating immune cells. T cells accounted for 21.65% in reRCC and 40.16% in pRCC, while monocytes accounted for 9.53% in reRCC and 19.81% in pRCC. The proportion of vascular endothelial cells in reRCC and pRCC was 7.46% and 8.28%, respectively, indicating the rationality of antiangiogenic therapy in RCC. Remarkably, compared with normal and pRCC samples, reRCC samples harbored a relatively higher proportion of fibroblasts (51.29% vs 2.19%). The infiltration levels of B cells, natural killer (NK) cells, and mast cells were relatively low in all patients.

In summary, all the described cell types were shared across patients, however, the proportion of cell types varied among pRCC and reRCC patients, revealing substantial heterogeneity of their TME compositions (figure 1E,F).

Identification and characterization of malignant cells in PRCC and reRCC

In this study, we identified four main subtypes of epithelial cells in adjacent normal kidneys, pRCC, and reRCC tissues. Thereafter, copy number variation (CNV) analysis was performed to distinguish between malignant and non-malignant epithelial cells (online supplemental figure S1A). CNVs accumulated in most tumor-derived epithelial cells and showed high heterogeneity among clusters. Our data also indicated that the average CNV level of each epithelial cell in tumor samples was significantly higher than that in normal samples (figure 2A). We further employed K-Means clustering in all epithelial cells to distinguish between malignant and non-malignant epithelial cells based on CNV levels. K-Means clustering revealed seven distinct classes of expression patterns. The results showed a lower CNV score in class 3 and class 5, which were mainly composed of epithelial cells derived from normal samples. When class 3 and class 5 were split by groups, an extremely lower CNV score was found in the normal groups (online supplemental figure S1B,C). Therefore, we defined epithelial cells derived from the adjacent normal kidney in class 3 and 5 as non-malignant epithelial cells, and the rest as malignant cells. A significantly higher CNV score was characterized in malignant cells (figure 2B,C).

We further examined the differentially expressed genes (DEGs) in malignant cells between pRCC and reRCC samples (online supplemental table S5). We found that the expression of CXCR4 was significantly higher in malignant cells in pRCC patients (figure 2D). CXCR4 is considered as an oncogene that promotes tumor progression and has been reported as a new therapeutic target for RCC.[38] MIF, LDHA, and ENO1 were also found upregulated in pRCC (figure 2D). HALLMARK pathways analysis of upregulated expression genes enriched in oxidative phosphorylation and hypoxia suggested a hypoxic characteristic in pRCC (figure 2E). The genes upregulated in malignant cells in reRCC included VCAN, LUM, and POSTN (figure 2D). Pathway enrichment analysis based on HALLMARK gene sets indicated a highly activated state of epithelial-mesenchymal transition and angiogenesis pathways in reRCC patients (figure 2F).

These results showed the heterogeneity in expression pattern and difference in activated pathways between reRCC and pRCC in malignant cells.

CD8$^+$T cells had a lower infiltrating level and were enriched in the apoptosis pathway in reRCC

The re-clustering of T cells revealed seven clusters, including 1 cluster of Tregs (CD4$^+$, FOXP3$^+$), three clusters of Th1/Th17 cells (CD8$^-$, IL7R$^+$), and three clusters of CD8$^+$ T cells (CD8A$^+$ IL7R$^+$, CD8A$^+$ GZMH$^+$ IL7R$^-$, and CD8A$^+$ HAVCR2$^+$) (figure 3A and online supplemental figure S2A). These subtypes were present in all pRCC and reRCC samples (figure 3B). Tregs presented in tumors and displayed increased expression of CD4, FOXP3, and LAIR2 (figure 3B, and online supplemental figure S2B). All 3 subtypes of CD8$^+$ T cells showed increased expression of cytotoxic genes GZMK, GZMA, and NKG7 (online supplemental figure S2C). Cluster 0 of CD8$^+$ T cells (CD8A$^+$ IL7R$^+$ cells) was characterized by specifically expressing IL7R and was previously reported to be precursors of memory CD8$^+$ T cell.[39] Cluster 1 of CD8$^+$T cells (CD8$^+$ GZMH$^+$ IL7R$^-$ cells) displayed a high expression of the cytotoxic genes GZMH, GZMK, GZMA and NKG7, and low expression of all checkpoint genes and IL7R, which was similar to the T cell subtype previously described by Zheng *et al*[40]; suggesting that these cells are precursors of cytotoxic T cells (online supplemental figure S2C). Cluster 4 (CD8A$^+$ HAVCR2$^+$ cells) in CD8$^+$ T cells highly expressed genes associated with cytotoxicity (GZMA, GZMB, and GZMK) and exhaustion-related markers (TIGHT, HAVCR2, and LAG3), suggesting that these cells are exhausted CD8$^+$ T cells (online supplemental figure S2C). Moreover, the total fraction of CD8$^+$T subtypes tended to be more abundant in pRCC versus reRCC (19.6% vs 9.4% of total cells, p=0.09, figure 3B). We then validated that the infiltrating level of CD8$^+$T cells

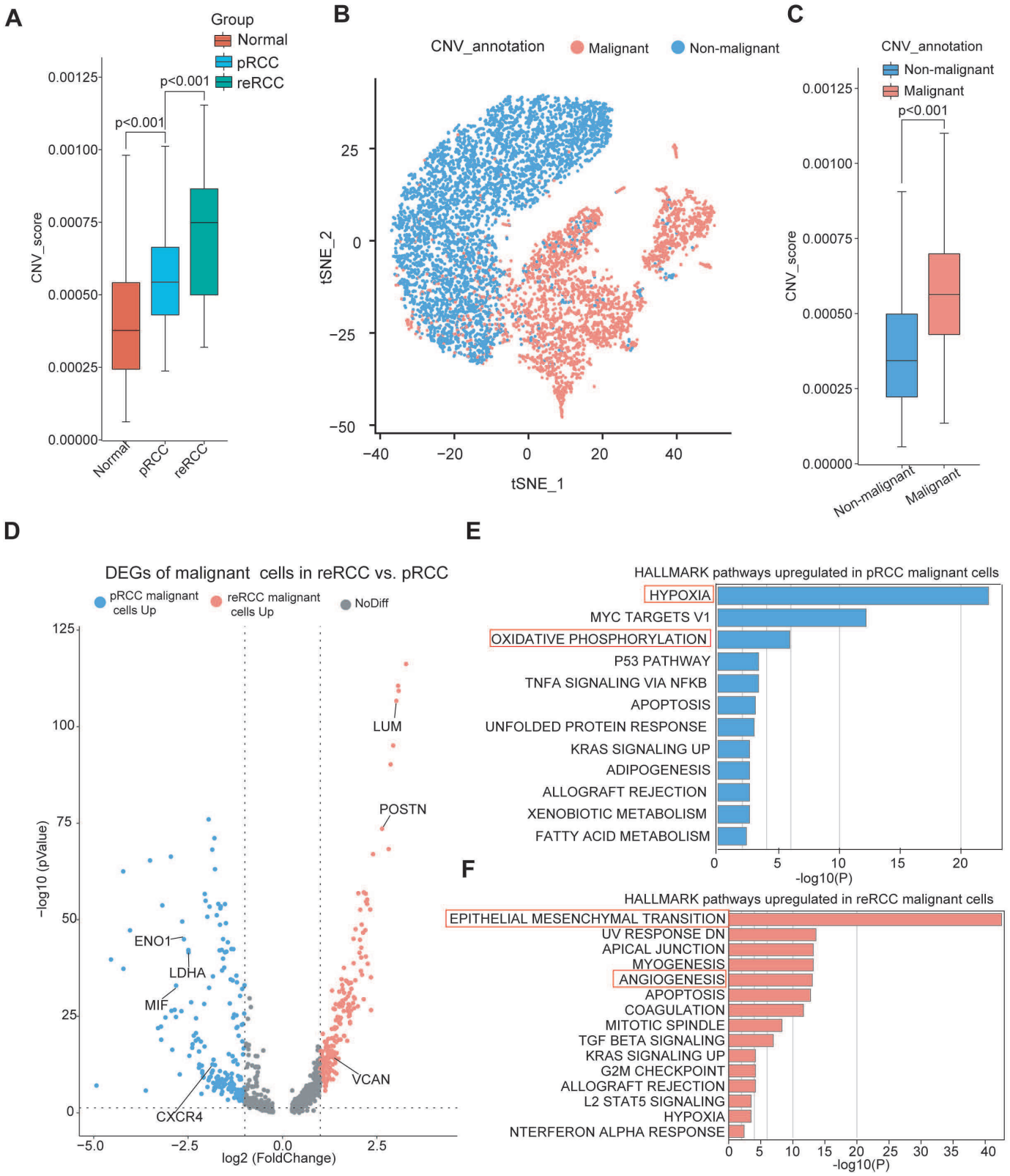

Figure 2 Identification and characterization of malignant cells in pRCC and reRCC. (A) CNV score of epithelial cells in normal, pRCC and reRCC tissues. (B) The t-SNE plot, showing the malignant and non-malignant epithelial cells. (C) CNV score of malignant and non-malignant epithelial cells. (D) The volcano plot shows DEGs between pRCC (blue dots) and reRCC malignant cells (red dots). (E, F). Bar chart showing the enrichment of specific pathways, based on the HALLMARK gene set of upregulated genes of malignant cells in reRCC (E) and pRCC. CNV, copy number variation; DEGs, differentially expressed genes; pRCC, primary renal cell carcinoma; reRCC, recurrent renal cell carcinoma; t-SNE: T-distributed stochastic neighbor embedding.

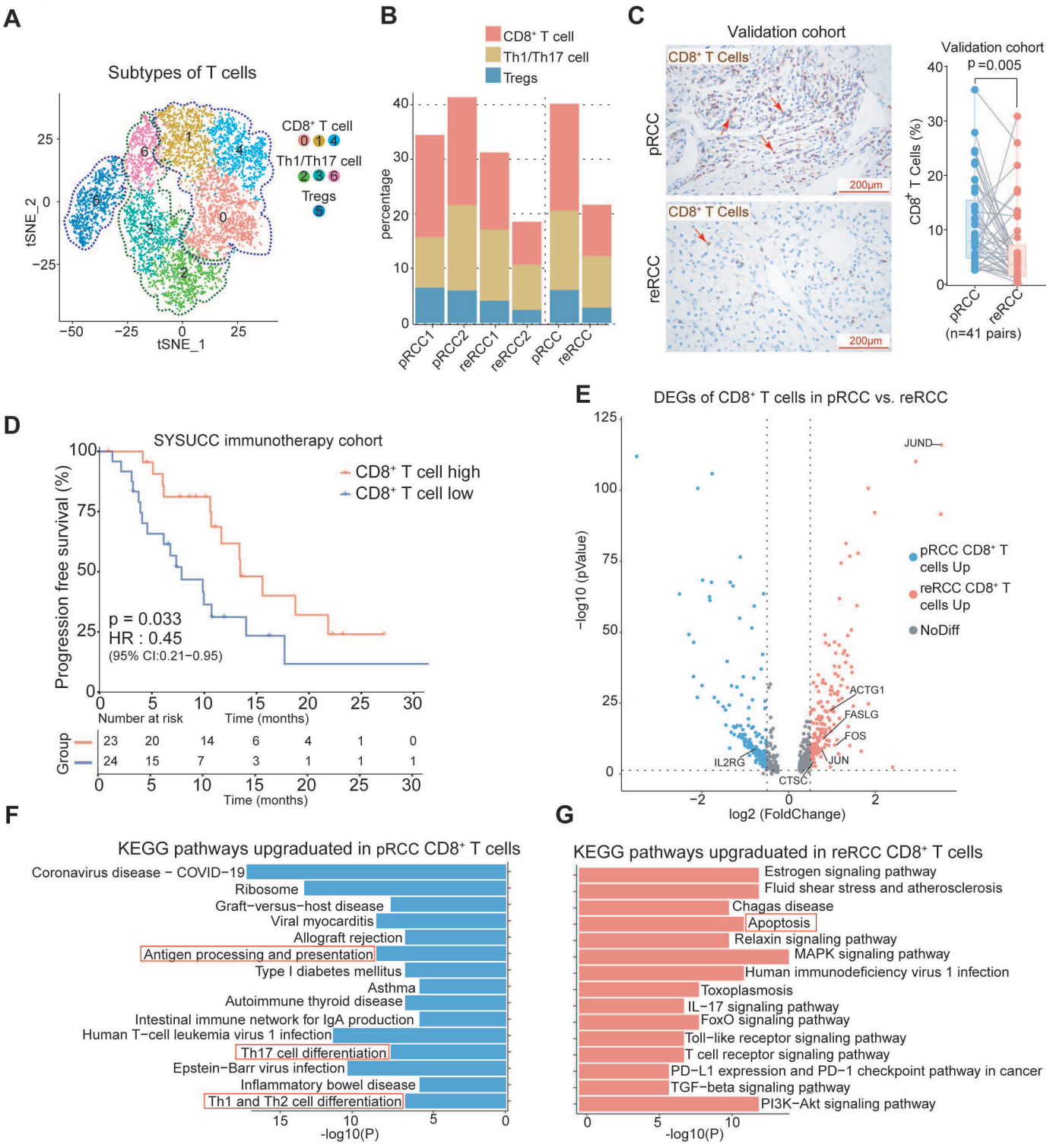

Figure 3 Characteristics of infiltrating T cell in pRCC and reRCC. (A) The t-SNE plot, showing subclustered T cells, is labeled in different colors. Cell type annotations are provided in the figure. (B) Histogram showing the percentage of T cell subtypes in samples and groups. (C) IHC staining of CD8A antibodies, showing the infiltration of CD8$^+$ T cells, in paired pRCC and reRCC samples from the validation cohort. Scale bars, 50 μm. (D) PFS curves according to CD8$^+$ T cells infiltration in tumor tissues in SYSUCC immunotherapy cohort. CD8 high represented a higher CD8$^+$ T cells infiltration and showed a significantly better prognosis. (E) The volcano plot shows differentially expressed genes between pRCC (blue dots) and reRCC CD8$^+$ T cells (red dots). (F, G) Bar chart showing the enrichment of specific pathways, based on the KEGG gene set of upregulated genes, in pRCC and reRCC CD8$^+$ T cells. IHC, immunohistochemistry; PFS, progression-free survival; pRCC, primary renal cell carcinoma; RCC, renal cell carcinoma; reRCC, recurrent renal cell carcinoma; SYSUCC, Sun Yat-sen University Cancer Center; t-SNE, T-distributed stochastic neighbor embedding.

was significantly higher in pRCC than in reRCC via IHC staining of 41 pairs of pRCC and reRCC samples from the validation cohort (mean:11.02% vs 6.42% of total cells, p=0.005; figure 3C). Furthermore, we found that a high infiltrating level of CD8+T cells was significantly associated with longer PFS in RCC patients who received immunotherapy in the SYSUCC immunotherapy cohort (HR 0.45, p=0.033, figure 3D). In the TCGA cohort, higher CD8+T cells infiltration was associated with better overall survival (OS) (HR 0.58, p<0.001) and PFS (HR 0.6, p<0.001) in RCC patients (online supplemental figure S2D).

DEGs analysis between pRCC and reRCC indicated that IL2RG was significantly upregulated in CD8+T cells in pRCC tissues (figure 3E; online supplemental table S6). Protein γc (encoded by IL2RG) was regarded as a component of the receptor for multiple cytokines, including IL-2, IL-4, IL-7, IL-9, IL-15 and IL-21, which could drive T cell proliferation and differentiation.[41] KEGG pathway analysis showed that CD8+T cells in pRCC were characterized by upregulated T cell differentiation, antigen processing and presentation (figure 3F) whereas the upregulated genes of CD8+T cells in reRCC tissues were characterized by apoptosis-related genes such as JUN, FOS, FASLG, ACTG1 and CTSC (figure 3E; online supplemental table S6). We also found that the apoptotic pathway was upregulated in CD8+T cells of reRCC samples (figure 3G).

In summary, by analyzing the proportion and activated pathways in pRCC and reRCC, we observed a superior anti-tumor immunity of CD8+T cells in pRCC than in reRCC tissues.

Progressive dysfunction of CD8+T cells in RCC by trajectory analysis

We explored the dynamic immune states and gene expression of RCC-infiltrated CD8+T cells by inferring the state trajectories using Monocle. Most of the CD8+T cells were found to be derived from pRCC and showed a high-density peak at both the early and end-stage of pseudotime (figure 4A). We then performed clustering of the genes with pseudotemporal expression pattern, whereby the ordering of genes was clustered into five clusters. Genes in cluster 1, including FASLG, SFRP2 and MEF2C, were highly expressed at the end stage and GO analysis suggested that their function mainly enriched the inflammatory cell apoptotic process, extrinsic apoptotic signaling pathway via death domain receptors, and negative regulation of cell migration. Genes in cluster 2 tended to be downregulated during the pseudotime. GO enrichment analysis showed that their functions were enriched in a series of immune activation functions, such as T cell activation, positive regulation of cytokine production, T cell proliferation, leukocyte mediated cytotoxicity and immune response-activating signal transduction (figure 4B,C).

To further investigate the transition states associated with CD8+T cells in reRCC and pRCC samples, we separately analyzed the trajectories of CD8+ T cells in pRCC and reRCC samples. CD8+T cells in reRCC samples were primarily allocated at the terminal ends in pseudotime trajectories (figure 4A). We next investigated the cytotoxicity changes associated with transitional states. Cytotoxicity-related genes including PRF1, IFNG, CST7, TNFSF10, NKG7, GZMB, and GZMA in CD8+ T cell in both pRCC and reRCC samples tended to be downregulated during the pseudotime (figure 4D).

In short, CD8+ T cells were progressively dysfunctional with gradually reduced cytotoxicity and increased apoptotic trend, which indicated an immune tolerance status during pseudotime trajectories in pRCC and reRCC.

CAFs' expression pattern and clinical outcomes in RCC patients

Our scRNA-seq data revealed that compared with pRCC, the infiltrating proportion of CD8+ T cells tended decreased and the abundance CAFs tended to be increased in reRCC (figure 1E). By performing IHC staining assay in paired pRCC and reRCC samples, we verified the infiltration of CAFs was significant higher in reRCC samples (12.5% vs 5.2 %, p<0.001, figure 5A). Moreover, we found that CD8+ T cells infiltration was negatively correlated with the CAFs infiltrating abundance using IHC staining (r=−0.21, p=0.02) (figure 5B). This led us to hypothesize that the low degree of CD8+ T cells infiltration in reRCC could be caused CAFs. We coculture the CAFs and CD8+ T cells on Matrigel.[42] The rate of apoptotic CD8+ T cells cocultured with CAFs was increased compared with CD8+ T cells culture on Matrigel alone (15.12% vs 5.00 %, p<0.001, figure 5C). We then explored the prognosis significance in RCC patients in SYSUCC immunotherapy cohort and TCGA RCC cohort. A high infiltrating level of CAFs was significantly associated with a poorer PFS in RCC patients who received immunotherapy in the SYSUCC immunotherapy cohort (HR 2.27, p=0.031, figure 5D). Analogously, in the TCGA RCC cohort, higher CAFs infiltration was associated with worse OS (HR 1.49, p=0.011) and PFS (HR 1.44, p=0.007, online supplemental figure S3A).

To further explore the potential mechanism of promoting tumor progression and immunotherapy resistance of CAFs, we investigated the expression pattern of CAFs. Recluster of CAFs identified seven clusters, including five clusters of myo-CAFs (mCAFs) and two clusters of inflammatory CAFs (iCAFs) according to the expression of RGS5 (mCAFs) and PDGFRA (iCAFs)[43] (figure 5E,F). Interestingly, we identified significantly increased expression of LGALS1(Gal1) in CAFs (figure 6A), which was widely reported as an immunosuppressive factor that could induce T cell apoptosis.[17 18 21 44] Then, we noticed that LGALS1 was highly expressed in all seven subtypes of fibroblast (online supplemental figure S3B). To further verify the expression of LGALS1 in CAFs, we isolated and cultured primary CAFs from RCC patients and using multiplexed immunofluorescent staining to confirm a high expression of α-SMA and Gal1(online supplemental figure S3C,D). Next, we confirmed that Gal1 had a higher expression level in CAFs compared with human RCC cell

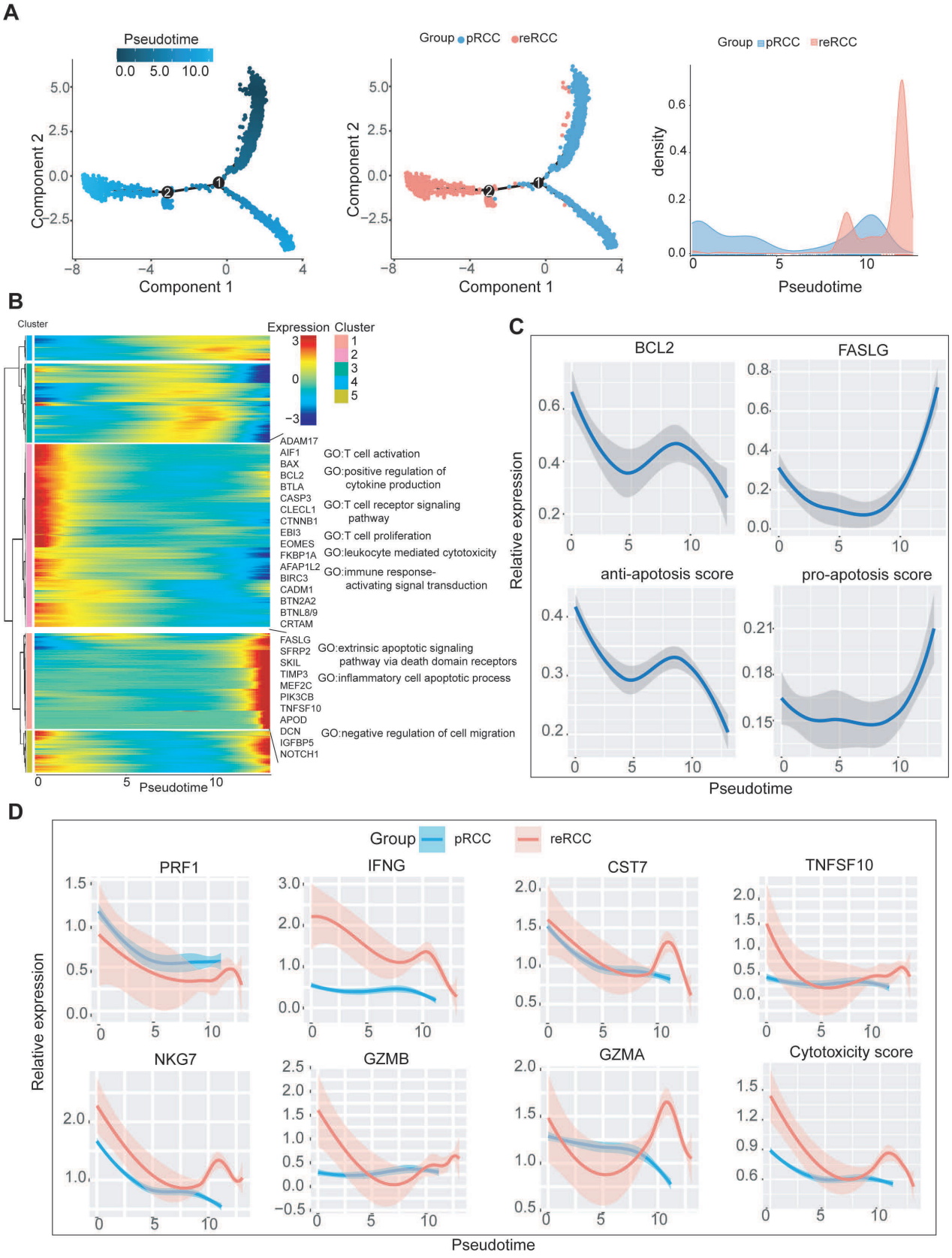

Figure 4 Analysis of CD8 +T cell transition states in pRCC and reRCC samples. (A) Pseudotime-ordered analysis of CD8$^+$ T cells from pRCC and reRCC samples. (B) Heatmap showing the dynamic changes in gene expression along the pseudotime. (C) Two-dimensional plots showing the expression scores for genes related to antiapoptosis and proapoptosis along with the pseudotime. (D) Two-dimensional plots showing the dynamic expression of cytotoxicity genes and cytotoxicity score during the CD8$^+$ T cell transitions along the pseudotime in pRCC (blue) and reRCC (red) samples. GO, gene ontology; pRCC, primary renal cell carcinoma; reRCC, recurrent renal cell carcinoma.

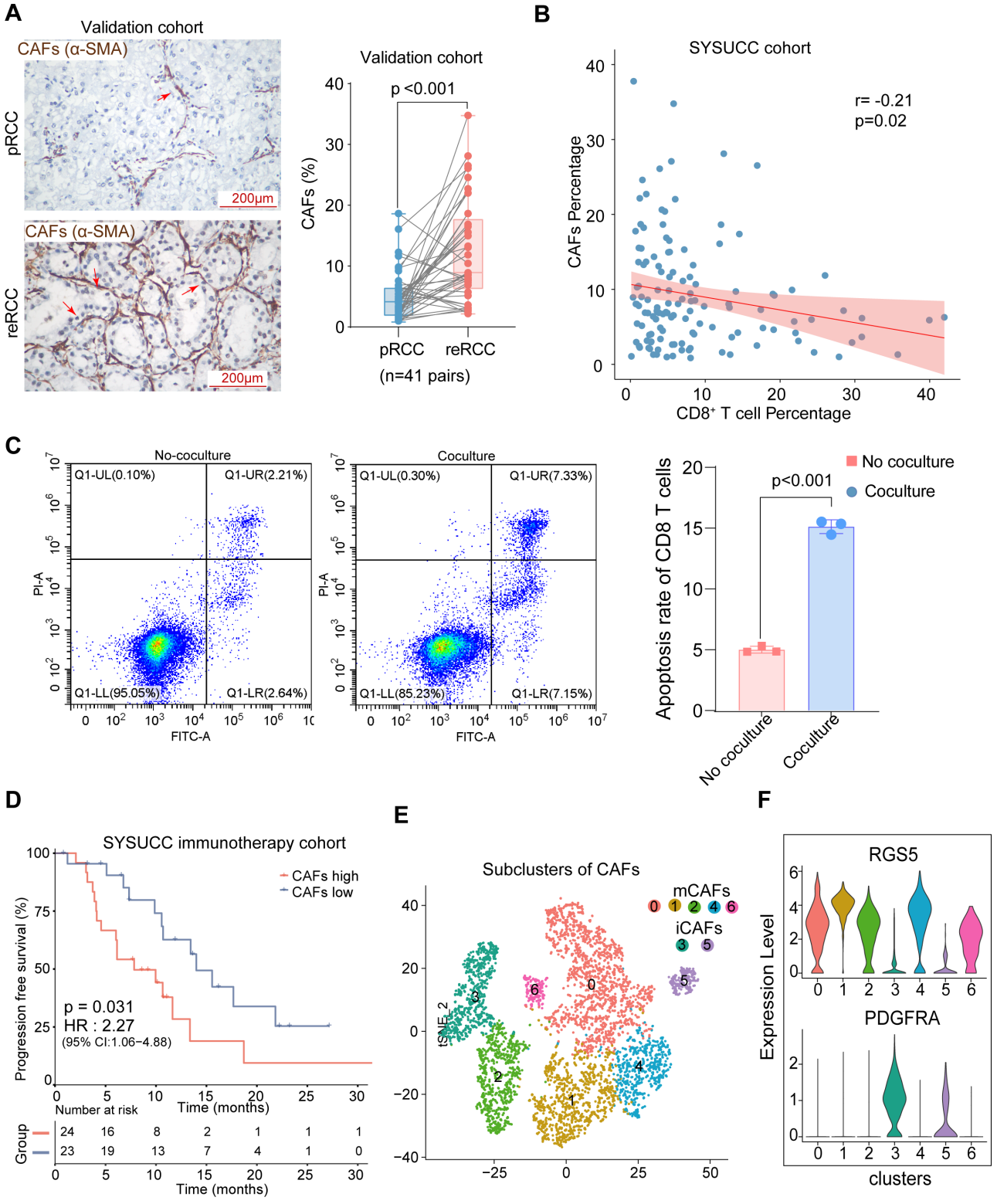

Figure 5 Expression pattern and clinical relevance of CAFs in RCC. (A) IHC staining of α-SMA (a marker of CAFs), in paired pRCC and reRCC samples from the validation cohort. Scale bars, 50 μm. (B) The correlation between IHC staining of α-SMA (a marker of CAFs) and IHC staining of CD8A in 129 RCC patients. (C) Flow cytometric analysis of the proportion of apotostic $CD8^+$ T cells, left, $CD8^+$ T cells did not coculture with CAFs; right, $CD8^+$ T cells cocultured with CAFs. (D) PFS curves according to CAFs (infiltration high or low groups) in tumor tissues in the SYSUCC immunotherapy cohort. The CAFs infiltration high group showed significantly worse PFS. (E) t-SNE projections of subclustered CAFs, labeled in different colors. Cell type annotations are provided in the figure. (F) Violin plots showing the markers of subtypes of CAFs. CAFs, cancer-associated fibroblasts; iCAFs, inflammatory cancer-associated fibroblasts; IHC, immunohistochemistry; mCAFs, Myo-cancer-associated fibroblasts; PFS, progression-free survival; pRCC, primary renal cell carcinoma; reRCC, recurrent renal cell carcinoma; SYSUCC, Sun Yat-sen University Cancer Center; t-SNE, T-distributed stochastic neighbor embedding.

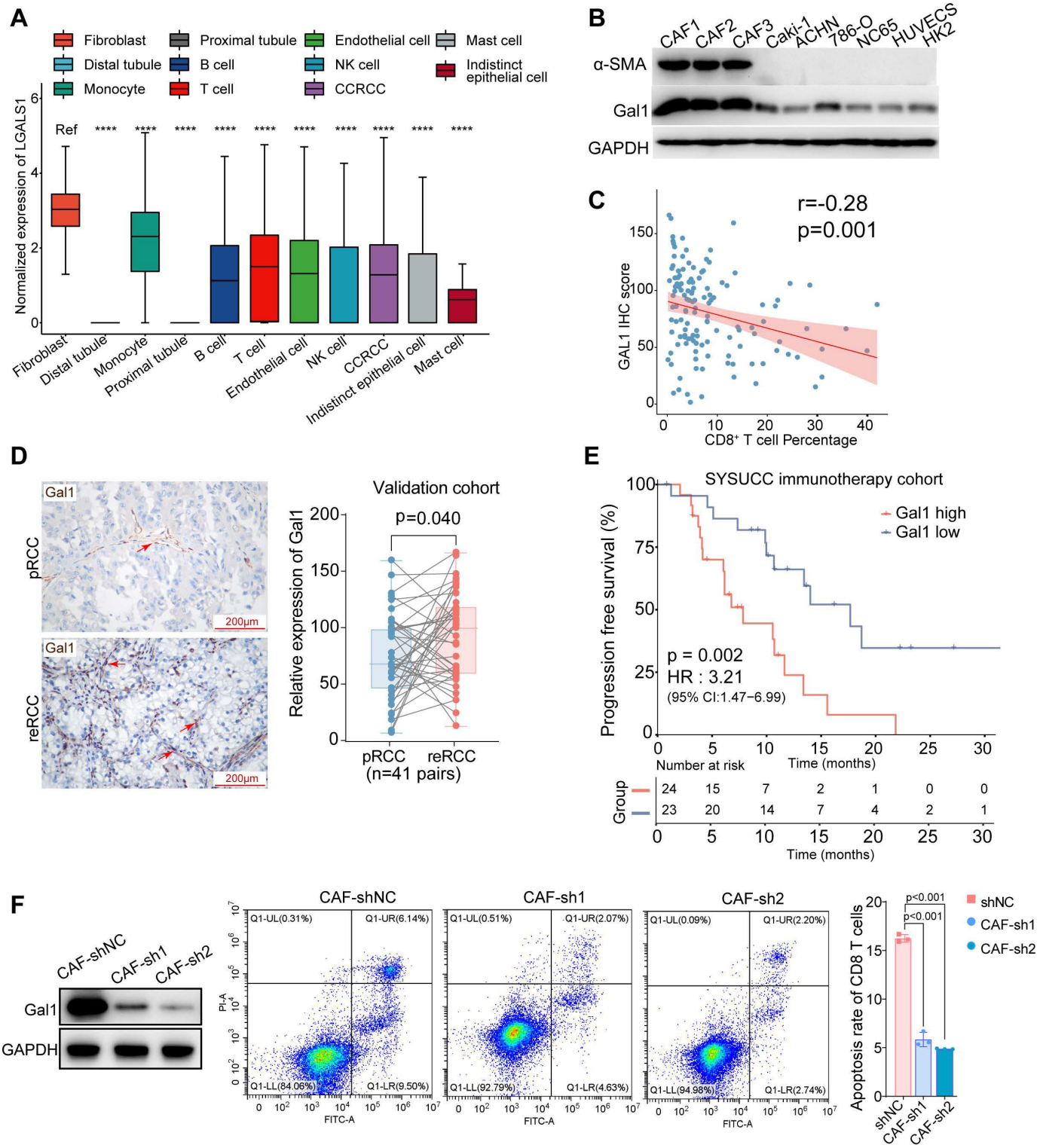

Figure 6 CAFs induced CD8⁺ T cells apoptosis via Gal1. (A) Box plots showing LGALS1 (Gal1) highly expressed in CAFs, compared with other types of cells. (B) Western blotting of α-SMA and Gal-1 in primary CAFs and human RCC cell lines (Caki-1, ACHN, 786-O, and NC65), vein endothelial cell line HUVEC, human kidney cortex/proximal tubule cells (HK2). (C) The correlation between IHC staining of Gal1 and CD8A in 129 RCC patients. (D) IHC staining of Gal1 in paired pRCC and reRCC samples from the validation cohort. Scale bars, 50 μm. (E) PFS curves according to Gal1 (expression high or low groups) in tumor tissues in the SYSUCC immunotherapy cohort. A high expression of Gal1 was significantly associated with a worse PFS. (F) Flow cytometric analysis of the proportion of apotostic CD8⁺ T cells cocultured with control CAFs and Gal1 knock-down CAFs. CAFs, cancer-associated fibroblasts; IHC, immunohistochemistry; PFS, progression-free survival; pRCC, primary renal cell carcinoma; reRCC, recurrent renal cell carcinoma; SYSUCC, Sun Yat-sen University Cancer Center.

lines (Caki-1, ACHN, 786-O, and NC65), vein endothelial cell line HUVEC, human kidney cortex/proximal tubule cells (HK2) by Western Blotting (figure 6B). We found that lower $CD8^+$ T cells infiltration was correlated with higher expression level of Gal1 (figure 6C). Gal1 was expressed higher in reRCC samples than in pRCC samples (figure 6D). For clinical significance, a high expression level of Gal1 was significantly associated with a worse PFS in RCC patients in the SYSUCC immunotherapy cohort (HR 3.21, p=0.002, figure 6E). Further, a high expression level of LGALS1 was associated with a poorer OS (HR 1.71, p<0.001) and PFS in RCC patients in the TCGA cohort (HR 1.88, p<0.001, online supplemental figure S3E).

To investigate that CAFs could trigger $CD8^+$ T cells apoptosis via Gal1, we established Gal1 knockdown CAFs (CAF-sh1 and CAF-sh2) cell lines (figure 6F). When $CD8^+$ T cells cocultured with Gal1 knockdown CAFs (CAF-sh1 and CAF-sh2) on Matrigel, the rate of apoptotic $CD8^+$ T cells was decreased, compared with $CD8^+$ T cells cocultured with control CAFs (5.85% vs 16.08%, 5.41% vs 16.08%, p<0.001, figure 6F).

We thereby concluded that immunosuppressor Gal1 was substantially expressed in CAFs. Upregulation of Gal1, as well as abundant CAFs, predicted a poor prognosis in RCC patients receiving immunotherapy. And CAFs could trigger $CD8^+$ T cells apoptosis by Gal1.

CAFs promote tumor growth and hamper immunotherapy efficacy by expressing Gal1 in vivo

To further evaluate the relationship between Gal1 expressed in CAFs and immunosuppression, in vivo experiments were performed in immune-competent BALB/c mice. We knocked down Gal1 in NIH/3T3 cell line, as shRNA2 had better efficiency in knocking down Gal1 expression (online supplemental figure S3F), we labeled NIH/3T3 cell transduced with shRNA2 as NIH/3T3(shGal1). Luciferase-expressing mouse-derived cell line (Renca-luc) and NIH/3T3(shGal1) were used for these experiments. We established two groups: cancer cells (Renca -luc) plus NIH/3T3 (shNC) as the control group, and cancer cells plus with Gal1 knocked down NIH/3T3 (Renca-luc +NIH/3T3(shGal1)) as the research group. Cancer cells and fibroblasts were inoculated into the left kidney cortex of each mouse, and tumor growth was assessed using a bioluminescent imaging system (IVIS). Orthotopic tumors were harvested after 4 weeks, and tumor volume analysis revealed that tumors were significantly smaller when Gal1 level was knocked down in NIH/3T3 cells in BALB/c mice (p=0.018, figure 7A). These results suggested that CAFs could promote tumor growth by expressing Gal1. To further assess whether knocking down Gal1 could influence the $CD8^+$ T cell infiltration and apoptosis, we tested the abundance and apoptosis of infiltrating $CD8^+$ T cells in the orthotopic tumors of the two groups in BALB/c mice by multiplexed immunofluorescence staining for CD8A and TUNEL. In mice implanted with Renca-luc plus NIH/3T3-shGal1, the infiltrating level of $CD8^+$ T cells was significantly higher (17.62% vs 12.59%, p=0.02, figure 7B) and the ratio of apoptotic $CD8^+$ T cells was significantly decreased (5.76% vs 12.12%, p=0.02, figure 7B), compared with the group implanted with Renca-luc plus NIH/3T3(shNC). These in vivo data further supported that CAFs could promote tumor growth and induce $CD8^+$ T cell apoptosis by expressing Gal1.

Next, we investigated whether Gal1 expression level in CAFs could impact the antitumor effect of anti-PD1 in vivo. Renca +NIH/3T3(shGal1) or Renca +NIH/3T3(shNC) cells were subcutaneously injected into the right flank of BALB/c mice. Our findings showed that tumor volume and weight were significantly lower when Gal1 was knocked down in NIH/3T3 (p<0.05, figure 7C). These results showed that knocking down Gal1 in NIH/3T3 substantially improved the tumor growth inhibition effect of anti-PD1 therapy in vivo.

Gal1 Specific inhibitor (OTX008) combined with anti-PD-1 enhanced the efficacy of immunotherapy in vivo

BALB/c mice subjected to subcutaneous injection of Renca +NIH/3T3(shNC) cells were randomly divided into four groups: (1) control, (2) OTX008 alone, (3) anti-PD1 alone, and (4) combined OTX008 and anti-PD1. The results showed a significant reduction in tumor growth compared with the control when administered with OTX008 alone (p<0.05), anti-PD1 alone (p<0.001), and the combined treatment (p<0.001). Interestingly, the combination of OTX008 and anti-PD1 exerted the most potent effect in inhibiting tumor growth. (figure 7D).

DISCUSSION

Recurrent tumors are often treated based on the molecular and pathological features of the primary tumor, especially in patients who have lost the opportunity for surgical resection or inability to obtain pathological specimens. However, studies comparing primary versus recurrent tumors suggested that secondary tumors can be extremely different from the primary tumor.[34 45] Sun *et al* described a distinctly different TME between primary and relapse hepatocellular carcinoma using scRNA-seq.[26] However, the difference in expression pattern and TME between pRCC and reRCC remained undeciphered. Given the high heterogeneity and the poor prognosis of advanced RCC patients, including reRCC, it is necessary to investigate the difference between pRCC and reRCC as precisely as possible.

In this study, we observed that reRCC was characterized by abundant CAFs and low numbers of $CD8^+$ T cells infiltration in the TME using scRNA seq data and validated the results by IHC staining in 41 paired pRCC and reRCC samples. There was a negative correlation between $CD8^+$ T cells and CAFs infiltration abundance. Remarkably, we identified that LGALS1 (Gal1), a well-known immunosuppressor,[17 18] was highly expressed in CAFs in RCC, especially in reRCC. And Gal1 expression in RCC

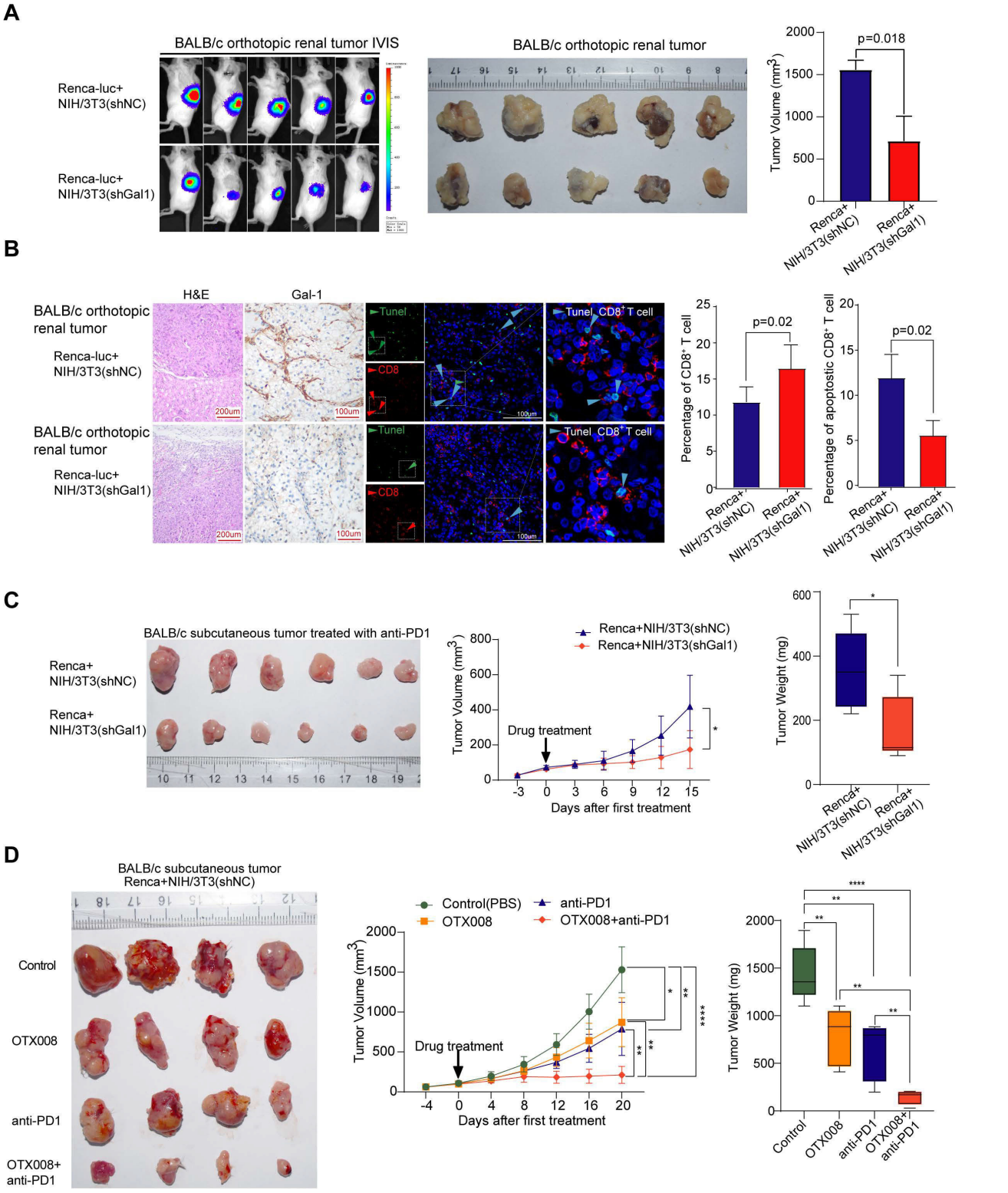

Figure 7 Gal1 inhibition reduces CD8⁺ T cells apoptosis and enhances immunotherapy efficacy in RCC model. (A) IVIS imaging of orthotopic renal tumors of Renca-luc cells cocultured with Gal1 -knocked-down NIH/3T3 (shGal1) fibroblasts, or Renca-luc cells cocultured with negative control NIH/3T3 (shNC) fibroblasts in BALB/c mice. Barplot showing the volume of tumors (right). (B) H&E staining (left). IHC staining of Gal1(middle), multiple immunofluorescence staining of CD8A and TUNEL(right) in orthotopic renal tumors from BALB/c mice. Barplot showing the percentage of infiltrating CD8⁺ T cells and the ratio of apoptotic CD8⁺ T cells to total CD8⁺ T cells. (C) Tumor growth curve for Renca cells plus NIH/3T3 (shNC) or Renca cells plus NIH/3T3 (shGal1) tumors treated with anti-PD1 antibody (n=6 mice/group). (D) Tumor growth curve for Renca cells plus NIH/3T3 (shNC) treated with PBS, OTX008, anti-PD1 antibody, and OTX008 combined anti-PD1 antibody (n=4 mice/group). Data are presented as the mean±SD. *P<0.05, **p<0.01, ****p<0.0001. IHC, immunohistochemistry; IVIS, bioluminescent imaging system; PBS, phosphate-buffered saline.

was significantly correlated with CD8+ T cells infiltration. By coculture experiments, we indicated that CAFs could trigger CD8+ T cells apoptosis by Gal1. Clinically, we found that high infiltrating level of CD8+ T cells was associated with better prognosis, whereas upregulation of Gal1, as well as abundant CAFs, was associated with poor PFS in RCC patients who received immunotherapy. In vivo, knocking down Gal1 in CAFs could suppress tumor growth, increase CD8+ T cells infiltration, reduce the proportion of apoptotic CD8+ T cells, and enhance the efficacy of immunotherapy. We elucidated that the combinational treatment of anti-PD1 with OTX008, the specific inhibitor of Gal1,[46] could improve immunotherapy efficacy compared with those administered with anti-PD1 alone.

Our data showed reduced CD8+ T cells infiltration in the TME of reRCC. This indicated that reRCC could be characterized as a cold tumor, which is defined by a low degree of T cell and CD8+ T cell infiltration and the downregulation of immune checkpoints such as PD-1, PD-L1, and LAG3(48). CD8+ T cells play a central role in anti-tumor immunity, and clinical evidence has proved that cold tumor was poorly responsive to immunotherapy.[11] Whereas immunotherapy could be more effective in hot tumors, which are characterized as having high CD8+ T cell density.[15 47 48] In renal clear cell carcinoma, baseline CD8 +T cell infiltration does not predict response to immunotherapy,[49 50] however, the lack of an association between PFS in RCC patients received immunotherapy and the presence of CD8+ cells should not be interpreted to indicate that these elements are irrelevant but more likely indicate that other factors are also contributing to biological responses to immunotherapy.[50] In the phase 3 JAVELIN Renal 101 trial,[50] although no association between PFS and CD8+ cells detected by IHC in tumor region was observed in the combination arm (avelumab plus axitinib), their gene expression deconvolution results indicated that CD8+ T cells had a significant interaction term with PFS in patients received avelumab plus axitinib, which further reinforce the clinical significance of cytotoxic T cells in advanced RCC. In our study, increased CD8+ T cell infiltration was associated with longer PFS (HR 0.45, p=0.033), compared with patients with lower CD8+ T cell infiltration. Similar results were found in our analysis of the TCGA-KIRC cohort.

Meanwhile, we found a high level of CAFs infiltration in reRCC. CAFs is an important contributor of ECM structure and have multiple ways to promote tumor progression.[16] CAFs could remodel the immunosuppressive tumor-infiltrating lymphocytes population of the TME by secreting a high level of IL-6 in esophageal cancer.[15] Interestingly, IL-6 secreted by CAFs could significantly enhance the malignancy of intrahepatic cholangiocarcinoma cells by promoting stem-like properties.[13] However, in our data, IL-6 had extremely low expression in CAFs as well as in other cell types in RCC (online supplemental figure S3G), which indicated the heterogeneity of CAFs among tumor types. In RCC, CAFs were highly prevalent cells in the TME and were involved in facilitating tumor cell proliferation, angiogenesis, metastasis, and therapy resistance.[51 52] Studies have shown that CAFs infiltrating the TME could hamper the response of immunotherapy in metastatic bladder, melanoma, and kidney cancer.[12 53] Based on the analysis of 47 patients who received immunotherapy in this study, significantly worse PFS was found in patients with high CAFs infiltration, compared with patients with low CAFs infiltration. Thus, our study provided additional evidence on immunotherapy resistance mediated by CAFs.

To further explore the potential mechanism of CAFs immunosuppression, the expression pattern of CAFs was investigated. Interestingly, we found that LGALS1 had highest expression level in CAFs among cell types in RCC. LGALS1 encodes the secretory protein Gal1, which is confirmed to promote tumor progression through a variety of mechanisms, such as angiogenesis,[54] epithelial-mesenchymal transformation,[24] and immunosuppression.[19 23] In 1995, Perillo *et al*[17] first reported that Gal1 induced apoptosis of activated human T cells in vitro. Our in vivo study showed that the ratio of apoptotic CD8+ cells was significantly reduced and the CD8+ T cells infiltration was increased in the tumor model implanted with Renca plus NIH/3T3(shGal1). However, a study conducted by Nambiar *et al*[23] indicated that Gal1 secreted by endothelium remodeled immunosuppression TME via T cell exclusion rather than apoptosis, and other reports showed inconsistencies in the Gal1 apoptotic effect depending on the tumor model.[44 55] And it was reported that stromal cell in ECM is able to directly kill susceptible T cells via Gal1.[42] In the coculture experiments in our study, when CD8+ T cells and CAFs cocultured together directly on Matrigel, the rate of apoptotic CD8+ T cells was increased and could be inhibited by Gal1 knockdown, which indicated that CD8+ T cell death was Gal1 dependent.

Immunotherapy has brought hope to patients with advanced RCC while the majority of patients still do not have durable responses to these agents,[7–9 33] and efficacy has been compromised in cases where CD8+ T cells infiltration is low.[15 47 48] In such cases, combination therapy strategies could be envisaged to both increase the CD8+ T cells infiltration and stimulate preexisting immune cell function. We found that knocking down Gal1 in CAFs could alter the TME from a cold tumor to a hot tumor, and enhance the efficacy of immunotherapy in vivo. These results implied the rationality of combination immunotherapy with targeting Gal1 in tumors with abundant infiltrating CAFs or overexpression of Gal1. In our study, we proved that OTX008 and anti-PD1 combination therapy could inhibit tumor growth in murine renal cancer models, compared with those treated with anti-PD1 alone. Furthermore, the specific inhibitor of Gal1, OTX008, has completed the first phase of its clinical trial (https://ichgcp.net/clinical-trials-registry/NCT01724320), which could facilitate the conduction of further clinical trials of OTX008 on RCC. Taking together, these findings provided novel insights into the

combination of immunotherapy with other drugs. Gal1 expression showed the potential to be a predictor for the efficacy of immunotherapy in RCC, and targeting Gal1 combined with immunotherapy could improve the prognosis of patients with RCC.

Despite the important findings observed in this study, there were some limitations to be clarified. First, the scRNA-seq data of primary tumor and adjacent normal kidney tissues was downloaded from public datasets, although we strictly referenced the methods of the original literature mentioned when preparing our own single-cell suspension of recurrent tumor tissues and minimized the batch effects during analysis. Second, the pRCC and reRCC samples for scRNA-seq were limited and unpaired, although we validated the results in 41 paired pRCC and reRCC samples, the results of scRNA-seq data need to be further validated. Third, we demonstrated a progressively dysfunctional state of $CD8^+$ T cells with gradually reduced cytotoxicity in RCC through trajectory analysis. However, given the importance of post-transcriptional regulatory mechanisms, the mRNA expression level may not provide a true reflection of the protein expression in $CD8^+$ T cells.[11] Finally, although our results could bring new insights into the combination of immunotherapy with OTX008, the efficacy of such regimens are yet to be validated in clinical trials.

Conclusion

Our study delineated the heterogeneity between pRCC and reRCC, described a low $CD8^+$ T cell and high CAFs infiltration TME in reRCC, and highlighted CAFs as a suppressor of $CD8^+$ T cell via expressing Gal1. Thus, targeting Gal1 could enhance immunotherapy response, and combinational treatment of anti-PD1 with OTX008 could improve immunotherapy efficacy. Our work provides a novel mechanism of CAFs in mediating an inhibitory immune microenvironment and sheds light on a unique approach to improve the results of immunotherapy in RCC.

Author affiliations
[1]Department of Urology, Sun Yat-sen University Cancer Center, Guangzhou, Guangdong, China
[2]State Key Laboratory of Oncology in South China, Collaborative Innovation Center for Cancer Medicine, Sun Yat-Sen University Cancer Center, Guangzhou, China
[3]Department of Urology, Huazhong University of Science and Technology Union Shenzhen Hospital, Shenzhen, Guangdong, China
[4]Department of Urology, Peking University First Hospital, Beijing, China
[5]Department of Urology, Shanghai Jiao Tong University School of Medicine Affiliated Renji Hospital, Shanghai, China
[6]Department of Urology, Sun Yat-sen University First Affiliated Hospital, Guangzhou, Guangdong, China
[7]Department of Urology, Central South University Third Xiangya Hospital, Changsha, Hunan, China
[8]Department of Nephrology, Southern Medical University Nanfang Hospital, Guangzhou, Guangdong, China
[9]Department of Pathology, Sun Yat-sen University Cancer Center, Guangzhou, Guangdong, China

Acknowledgements We thank professor Sarah Teichmann kindly provided the single cell RNA-seq data of adjacent normal kidney and primary renal carcinoma tissues, and we thank all patients who participated in this study.

Contributors Responsible for the overall content as guarantor: Z-L Z. Conception and design: Z-L Z and F-J Z. Provision of study materials or patients: Z-S H, J-W H, J-Y L, J-H L, N J, Y C, H H, S-J G and P D. Collection and assembly of data: Z L, Z-S W, N W, X-P Z, W-S W, and M-H D. Data analysis and interpretation: Y-L P, L-B X and K N. Manuscript writing: Y-L P, Z-H Z and C-P Y. All authors read and approved the final manuscript.

Funding This study was supported by the National Natural Science Foundation of China (No. 81972382 and 81872091) and the Natural Science Foundation for Distinguished Young Scholars of Guangdong Province (No. 2021B1515020077).

Competing interests There are no competing interests

Patient consent for publication Not applicable.

Ethics approval This study was performed in accordance with the ethical standards of the Helsinki Declaration and the ethical guidelines for Medical and Health Research Involving Human Subjects. Written informed consent was obtained for each of the participant patients. All cases were de-identified and personal identifiable details were removed from their case descriptions to ensure anonymity. This study was approved and reviewed by the Ethics Review Board of Sun Yat-sen University Cancer Center (SYSUCC). Mouse experiments were performed in a specific pathogen-free environment at the animal laboratory of the SYSUCC according to institutional guidelines, and all animal experimental protocols were approved and reviewed by the Ethics Review Committee for Animal Experimentation of SYSUCC. All experiments were performed in accordance with the guidelines and regulations indicated by these committees.

Provenance and peer review Not commissioned; externally peer reviewed.

Data availability statement Data are available on reasonable request. All the data used in this study could be available from the author Yulu Peng (E-mail: pengyl1@sysucc.org.cn).

ORCID iDs
Yu-Lu Peng http://orcid.org/0000-0002-5213-4655
Jun-Hang Luo http://orcid.org/0000-0002-5706-0990

REFERENCES

1 He W, Wu Z, Zu L, *et al*. Application of erector spinae plane block guided by ultrasound for postoperative analgesia in breast cancer surgery: a randomized controlled trial. *Cancer Commun* 2020;40:122–5.
2 Ferlay J, Colombet M, Soerjomataram I, *et al*. Cancer incidence and mortality patterns in Europe: estimates for 40 countries and 25 major cancers in 2018. *Eur J Cancer* 2018;103:356–87.
3 Rini BI. Campbell Sc Fau - Escudier B, Escudier B. Renal cell carcinoma. *Lancet*2009;373:1119–32.
4 Wei J-H, Feng Z-H, Cao Y, *et al*. Predictive value of single-nucleotide polymorphism signature for recurrence in localised renal cell carcinoma: a retrospective analysis and multicentre validation study. *Lancet Oncol* 2019;20:591–600.
5 Eggener SE, Yossepowitch O, Pettus JA, *et al*. Renal cell carcinoma recurrence after nephrectomy for localized disease: predicting survival from time of recurrence. *J Clin Oncol* 2006;24:3101–6.

6 Ohsugi H, Ohe C, Yoshida T, *et al*. Predictors of postoperative recurrence in patients with non-metastatic pT3a renal cell carcinoma. *Int J Urol* 2021;28:1060–6.
7 Choueiri TK, Powles T, Burotto M, *et al*. Nivolumab plus cabozantinib versus sunitinib for advanced renal-cell carcinoma. *N Engl J Med* 2021;384:829–41.
8 Lee C-H, Shah AY, Rasco D, *et al*. Lenvatinib plus pembrolizumab in patients with either treatment-naive or previously treated metastatic renal cell carcinoma (study 111/KEYNOTE-146): a phase 1b/2 study. *Lancet Oncol* 2021;22:946–58.
9 Motzer RJ, Escudier B, George S, *et al*. Nivolumab versus everolimus in patients with advanced renal cell carcinoma: updated results with long-term follow-up of the randomized, open-label, phase 3 CheckMate 025 trial. *Cancer* 2020;126:4156–67.
10 Binnewies M, Roberts EW, Kersten K, *et al*. Understanding the tumor immune microenvironment (TIME) for effective therapy. *Nat Med* 2018;24:541–50.
11 Philip M, Schietinger A. CD8$^+$ T cell differentiation and dysfunction in cancer. *Nat Rev Immunol* 2021 doi:10.1038/s41577-021-00574-3
12 Galbo PM, Zang X, Zheng D. Molecular features of cancer-associated fibroblast subtypes and their implication on cancer pathogenesis, prognosis, and immunotherapy resistance. *Clin Cancer Res* 2021;27:2636–47.
13 Zhang M, Yang H, Wan L, *et al*. Single-cell transcriptomic architecture and intercellular crosstalk of human intrahepatic cholangiocarcinoma. *J Hepatol* 2020;73:1118–30.
14 Chen X, Song E. Turning foes to friends: targeting cancer-associated fibroblasts. *Nat Rev Drug Discov* 2019;18:99–115.
15 Kato T, Noma K, Ohara T, *et al*. Cancer-associated fibroblasts affect intratumoral CD8$^+$ and FoxP3$^+$ T cells via IL6 in the tumor microenvironment. *Clin Cancer Res* 2018;24:4820–33.
16 Liu T, Han C, Wang S, *et al*. Cancer-associated fibroblasts: an emerging target of anti-cancer immunotherapy. *J Hematol Oncol* 2019;12:86.
17 Perillo NL, Pace KE, Seilhamer JJ, *et al*. Apoptosis of T cells mediated by galectin-1. *Nature* 1995;378:736–9.
18 Nguyen JT, Evans DP, Galvan M, *et al*. CD45 modulates galectin-1-induced T cell death: regulation by expression of core 2 O-glycans. *J Immunol* 2001;167:5697–707.
19 Rubinstein N, Alvarez M, Zwirner NW, *et al*. Targeted inhibition of galectin-1 gene expression in tumor cells results in heightened T cell-mediated rejection; a potential mechanism of tumor-immune privilege. *Cancer Cell* 2004;5:241–51.
20 Thijssen VL, Heusschen R, Caers J, *et al*. Galectin expression in cancer diagnosis and prognosis: a systematic review. *Biochim Biophys Acta* 2015;1855:235–47.
21 Ito K, Stannard K, Gabutero E, *et al*. Galectin-1 as a potent target for cancer therapy: role in the tumor microenvironment. *Cancer Metastasis Rev* 2012;31:763–78.
22 Orozco CA, Martinez-Bosch N, Guerrero PE, *et al*. Targeting galectin-1 inhibits pancreatic cancer progression by modulating tumor-stroma crosstalk. *Proc Natl Acad Sci U S A* 2018;115:E3769–78.
23 Nambiar DK, Aguilera T, Cao H, *et al*. Galectin-1-driven T cell exclusion in the tumor endothelium promotes immunotherapy resistance. *J Clin Invest* 2019;129:5553–67.
24 Chong Y, Tang D, Xiong Q, *et al*. Galectin-1 from cancer-associated fibroblasts induces epithelial-mesenchymal transition through β1 integrin-mediated upregulation of Gli1 in gastric cancer. *J Exp Clin Cancer Res* 2016;35:175.
25 Wu M-H, Hong H-C, Hong T-M, *et al*. Targeting galectin-1 in carcinoma-associated fibroblasts inhibits oral squamous cell carcinoma metastasis by downregulating MCP-1/CCL2 expression. *Clin Cancer Res* 2011;17:1306–16.
26 Sun Y, Wu L, Zhong Y, *et al*. Single-cell landscape of the ecosystem in early-relapse hepatocellular carcinoma. *Cell* 2021;184:404–21.
27 Ding S, Chen X, Shen K. Single-cell RNA sequencing in breast cancer: understanding tumor heterogeneity and paving roads to individualized therapy. *Cancer Commun* 2020;40:329–44.
28 Young MD, Mitchell TJ, Vieira Braga FA, *et al*. Single-cell transcriptomes from human kidneys reveal the cellular identity of renal tumors. *Science* 2018;361:594–9.
29 Kim K-T, Lee HW, Lee H-O, *et al*. Application of single-cell RNA sequencing in optimizing a combinatorial therapeutic strategy in metastatic renal cell carcinoma. *Genome Biol* 2016;17:80.
30 Krishna C, DiNatale RG, Kuo F, *et al*. Single-cell sequencing links multiregional immune landscapes and tissue-resident T cells in ccRCC to tumor topology and therapy efficacy. *Cancer Cell* 2021;39:662–77.
31 Zhang Y, Narayanan SP, Mannan R, *et al*. Single-cell analyses of renal cell cancers reveal insights into tumor microenvironment, cell of origin, and therapy response. *Proc Natl Acad Sci U S A* 2021;118 doi:10.1073/pnas.2103240118
32 Bi K, He MX, Bakouny Z, *et al*. Tumor and immune reprogramming during immunotherapy in advanced renal cell carcinoma. *Cancer Cell* 2021;39:649–61.
33 Braun DA, Street K, Burke KP, *et al*. Progressive immune dysfunction with advancing disease stage in renal cell carcinoma. *Cancer Cell* 2021;39:632–48.
34 Hill RM, Kuijper S, Lindsey JC, *et al*. Combined MYC and P53 defects emerge at medulloblastoma relapse and define rapidly progressive, therapeutically targetable disease. *Cancer Cell* 2015;27:72–84.
3535 Laehnemann D, Köster J, Szczurek E. 12 grand challenges in single-cell data science. *PeerJ Preprints* 2019.:7:e27885v3.
36 Hu J, Chen Z, Bao L, *et al*. Single-Cell transcriptome analysis reveals intratumoral heterogeneity in ccRCC, which results in different clinical outcomes. *Mol Ther* 2020;28:1658–72.
37 Liao J, Yu Z, Chen Y, *et al*. Single-cell RNA sequencing of human kidney. *Sci Data* 2020;7:4.
38 Vaishampayan UN, McDermott DF, Matrana MR, *et al*. A phase 1/2 study evaluating the efficacy and safety of the oral CXCR4 inhibitor X4P-001 in combination with axitinib in patients with advanced renal cell carcinoma. *J Clin Oncol* 2018;36:4510. doi:10.1200/JCO.2018.36.15_suppl.4510
39 Kaech SM, Tan JT, Wherry EJ, *et al*. Selective expression of the interleukin 7 receptor identifies effector CD8 T cells that give rise to long-lived memory cells. *Nat Immunol* 2003;4:1191–8.
40 Zheng C, Zheng L, Yoo J-K, *et al*. Landscape of infiltrating T cells in liver cancer revealed by single-cell sequencing. *Cell* 2017;169:1342–56.
41 Rochman Y, Spolski R, Leonard WJ. New insights into the regulation of T cells by gamma(c) family cytokines. *Nat Rev Immunol* 2009;9:480–90.
42 He J, Baum LG. Presentation of galectin-1 by extracellular matrix triggers T cell death. *J Biol Chem* 2004;279:4705–12.
43 Chen Z, Zhou L, Liu L, *et al*. Single-cell RNA sequencing highlights the role of inflammatory cancer-associated fibroblasts in bladder urothelial carcinoma. *Nat Commun* 2020;11:5077.
44 Büchel G, Schulte JH, Harrison L, *et al*. Immune response modulation by galectin-1 in a transgenic model of neuroblastoma. *Oncoimmunology* 2016;5:e1131378.
45 Ramaswamy V, Remke M, Bouffet E, *et al*. Recurrence patterns across medulloblastoma subgroups: an integrated clinical and molecular analysis. *Lancet Oncol* 2013;14:1200–7.
46 Astorgues-Xerri L, Riveiro ME, Tijeras-Raballand A, *et al*. OTX008, a selective small-molecule inhibitor of galectin-1, downregulates cancer cell proliferation, invasion and tumour angiogenesis. *Eur J Cancer* 2014;50:2463–77.
47 Hegde PS, Karanikas V, Evers S. The where, the when, and the how of immune monitoring for cancer immunotherapies in the era of checkpoint inhibition. *Clin Cancer Res* 2016;22:1865–74.
48 Ji R-R, Chasalow SD, Wang L, *et al*. An immune-active tumor microenvironment favors clinical response to ipilimumab. *Cancer Immunol Immunother* 2012;61:1019–31.
49 Braun DA, Hou Y, Bakouny Z, *et al*. Interplay of somatic alterations and immune infiltration modulates response to PD-1 blockade in advanced clear cell renal cell carcinoma. *Nat Med* 2020;26:909–18.
50 Motzer RJ, Robbins PB, Powles T, *et al*. Avelumab plus axitinib versus sunitinib in advanced renal cell carcinoma: biomarker analysis of the phase 3 javelin renal 101 trial. *Nat Med* 2020;26:1733–41.
51 Chakiryan NH, Kimmel GJ, Kim Y, *et al*. Geospatial cellular distribution of cancer-associated fibroblasts significantly impacts clinical outcomes in metastatic clear cell renal cell carcinoma. *Cancers* 2021;13 doi:10.3390/cancers13153743
52 Errarte P, Larrinaga G, López JI. The role of cancer-associated fibroblasts in renal cell carcinoma. An example of tumor modulation through tumor/non-tumor cell interactions. *J Adv Res* 2020;21:103–8.
53 Zheng X, Zeng D, Peng W, *et al*. Interaction between CAF and CD8+ T cells in non-small cell lung cancer affects prognosis and efficacy of immunotherapy. *J Clin Oncol* 2020;38:9536.
54 Thijssen VL, Griffioen AW. Galectin-1 and -9 in angiogenesis: a sweet couple. *Glycobiology* 2014;24:915–20.
55 Dias-Baruffi M, Zhu H, Cho M, *et al*. Dimeric galectin-1 induces surface exposure of phosphatidylserine and phagocytic recognition of leukocytes without inducing apoptosis. *J Biol Chem* 2003;278:41282–93.

Single-cell transcriptomics reveals a low T cell infiltrating state mediated by fibroblasts in recurrent renal carcinoma

Methods

Human subject

Two tumor tissues from patients diagnosed with local recurrent clear cell renal carcinoma (reRCC) in Sun Yat-Sen University Cancer Center (SYSUCC) were used for scRNA-seq. Three perioperatively primary renal cell carcinoma (pRCC) tissues were obtained during nephrectomy and used for isolation and culture of CAFs. Formalin-fixed paraffin-embedded (FFPE) tissue blocks of pairwise primary and recurrent RCC were collected from 41 patients in Sun Yat-Sen University Cancer Center(SYSUCC, n=21, Guangzhou, China), Peking University Third Hospital (n=11, Beijing, China), Shanghai Jiao Tong University affiliated Renji Hospital (n=3, Shanghai, China), The First Affiliated Hospital of Sun Yat-Sen University (n=2, Guangzhou, China), The Third Xiangya Hospital of Central South University (n=2, Changsha, China), Nanfang Hospital, Southern Medical University(n=2, Guangzhou, China) as the validation cohort. 47 RCC patients who received immunotherapy in our center were included in the SYSUCC immunotherapy cohort. We defined progression-free survival (PFS) as no progression/relapse after immunotherapy use. The available clinical features of the SYSUCC immunotherapy cohort are summarized in **supplementary table S1**.

DEGs and pathways analysis

Differentially expressed gene analysis between pRCC and reRCC was conducted using ‘‘FindMarkers’’ function, implemented in the Seurat package, with log-scaled fold change > 0.5 and p value < 0.05 (Wilcoxon Rank Sum test). Pathways of DEGs in malignant cells were explored using HALLMARK gene sets and KEGG gene sets were utilized in pathways enrichment of DEGs in $CD8^+$ T cells.

Samples collection and initial processing

reRCC tissues were obtained from two patients diagnosed with local relapsed clear cell renal cell carcinoma in SYSUCC. Samples were directly obtained from the operating room during surgery. We strictly referenced the methods described by Young et al.[1] when preparing our own single-cell suspension. Tissues were rinsed in HBSS (Gibco) until there was no visible blood then sliced into approximately 30 mm^3 pieces of tissue and digested for 30 min at 37°C with agitation in a digestion solution containing 25μg/mL Liberase TM (Roche) and 50μg/ml DNase (Sigma) in RPMI (Gibco). Sample dissociation solutions were filtered by a 70-μm cell strainer, washed with PBS, and live cells enriched using a Dead Cell Removal Kit (Miltenyi Biotec) as per manufactures instructions. The single-cell suspension was stained with 0.4% trypan blue (Thermo Fisher Scientific) to examine the concentration of live cells. Cell suspensions immediately proceed to single-cell library preparation.

Library preparation and sequencing

Cellular suspensions were loaded on a 10X Genomics GemCode Single-cell instrument that generates single-cell Gel Bead-In-EMlusion (GEMs). Libraries were generated and sequenced from the cDNAs with Chromium Next GEM Single Cell 3'Reagent Kits v3.1. Single-cell transcriptomic amplification and library preparation were performed by Genedenovo Biotechnology Co., Ltd (Guangzhou, China) using single-cell 3′ v3 (10X Genomics). The libraries were then pooled and sequenced across six lanes on an Illumina NovaSeq 6000 system (Illumina, Inc., San Diego, California, US). Pre-processing of scRNA-seq fastq files was conducted using Cell Ranger v3.0.2 (10X genomics). scRNA-seq reads were aligned to the hg19 reference genome (ref-version 3.0.0), and the count matrix of cell barcodes by genes used for downstream analysis was generated using the Cell Ranger count function with parameter–expect-cells=3000.

Public data Acquisition

The scRNA-seq count matrix of 2 pRCC and 3 adjacent normal kidney tissues described by Young et al.[1] were downloaded and used, as this is the first study characterizing pRCC using scRNA-seq. For the TCGA cohort, the expression matrix, along with the clinical information of the patients containing 539 tumor samples and 72 normal samples were downloaded from The Cancer Genome Atlas (TCGA, https://portal.gdc.cancer.gov/) Kidney Renal Clear Cell Carcinoma (KIRC) dataset. The EPIC package (1.1.5) [2] was used to calculate the infiltration abundance of $CD8^+$ T cells and CAFs in the TCGA cohort.

Single-cell gene expression quantification and subcluster detection.

Raw gene expression matrices were imported and processed using the Seurat R package (version 3.1.5) [3]. Low-quality cells were removed following 3 measurements: 1) cells had either fewer than 200 or over 6000 unique molecular identifiers (UMIs), over 20,000 or less than 200 expressed genes or over 15% UMIs derived from the mitochondrial genome, or over 2.5% UMIs derived from the erythrocytic genome; 2) cells had an average expression level of less than 2 for a curated list of housekeeping genes[4]; 3) cells had a co-expression of EPCAM and PTPRC. 4) Doublets were detected by DoubletFinder R package (version 2.0.3) [5]for single sample and manually detected the doublets in re-clustering the cell types. 7 seurat objects containing 2 reRCC and 2 pRCC and 3 normal samples were then merged, and batch effects were minimized using Harmony R package (version 1.0)[6]. Gene expression matrices of the remaining high-quality cells were normalized to the total cellular UMI counts. The normalized expression was scaled (scale. factor = 10,000) by regressing out the total cellular UMI counts and percentage of mitochondrial gene. Highly variable genes (top 2000) were extracted using the Seurat FindVariableGenes function. Then, we performed principal component analysis (PCA) analysis using high variable genes, and significant PCs (top 20) were selected to perform dimension reduction. Clusters were found using FindClusters function (dims.use = 1:20, resolution = 0.5). The tSNE analysis was used for dimension

reduction and visualization of gene expression[7].

CNV analysis

Initial CNVs were estimated by the expression levels of genes within each chromosome region using the inferCNV R package[8]. The CNVs of epithelial cells were calculated by expression level from scRNA-seq data for each cell with a cutoff of 0.1. We further employed K-Means clustering in all epithelial cells to distinguish malignant and non-malignant epithelial cells based on CNV scores. The CNV score of each cell was calculated as quadratic means of (CNV region -1). Then, we distinguished malignant depended on the class of K-Means and cells distribution in groups.

Pseudotime trajectory analysis

The cell lineage trajectory of $CD8^+$T was inferred using the Monocle2 R package[9]. We used the ‘‘differentialGeneTest’’ function to derive DEGs from each cluster and genes with a q-value < 0.01 were used to order the cells in pseudotime analysis. After the cell trajectories were constructed, we then identified the genes that varied according to pseudotime using the “differentialGeneTest” function in Monocle2 and used them to perform GO enrichment analysis. We used the average expression (measured by log2 (TPM + 1) of anti-apoptosis, pro- apoptosis related genes to define the anti-apoptosis and pro-apoptosis score for $CD8^+$ T cells. The anti-apoptosis and pro-apoptosis related genes were listed in **Supplementary Table S2**.

Isolation and culture of CAFs from RCC tissues.

Briefly, primary RCC tissues were obtained from the operating room during nephrectomy. Tissues were rinsed in HBSS (Gibco) until there was no visible blood then sliced into approximately 30 mm^3 pieces of tissue and digested for 30 min at 37°C with agitation in a digestion solution containing 25μg/ml Liberase TM (Roche) and 50μg/ml DNase (Sigma) in RPMI (Gibco). Sample dissociation solutions were

filtered by a 40-μm cell strainer and were neutralized with complete medium and centrifuged at 300g for 5 min. The cell pellet was suspended in Dulbecco's Modified Eagle Medium (DMEM) containing 10% selected fetal bovine serum (FBS) and 1 ng/ml basic fibroblast growth factor (bFGF, R&D Systems, Minneapolis, MN), 100 μg/ml penicillin, and 100 U/ml streptomycin (Invitrogen, NY, USA). The cells were grown in the culture dishes. After 48h, non-adherent cells were removed and washed twice with phosphate-buffered saline (PBS). Adherent fibroblasts were further incubated for 5-8 days until 80-90% confluence. Then, the mixed fibroblasts were labeled by α-SMA (Sigma, Cat: A2547, 1:100) and sorted by FACS to enrich CAFs. The CAFs were further expanded in the above medium (DMEM +10% FBS) and passage 5~10 CAFs were used in this study.

IHC analysis

After deparaffinization, slides were hydrated in alcohol and endogenous peroxidase activity was quenched for 30 min in 10% hydrogen peroxide. Antigen epitope retrieval was induced by microwave heating. To examine the expression pattern of candidate antibodies in RCC tissues, sections were immunostained with primary antibodies for 1 hour at 37°C. Then, enzyme-labeled goat anti-mouse/rabbit IgG polymer (Cat: PV-6000, ZSGB-BIO, Beijing) was added and incubated at room temperature for 20 minutes. The signal was detected using DAB (ZSGB-BIO, Beijing), following the protocol of the manufacturer. The counts of CAFs, $CD8^+$ T cells and the IHC score of Gal1was calculated by HALO software (Indicalab, New Mexico, USA). The antibodies were listed as follows: CD8A (Abcam, ab237710, 1:1000); α-SMA (Sigma, Cat: A2547, 1:800); (Gal1, NSJ bioreagents, Cat: R31653, 1:1000)

Western Blotting.

Western blotting was performed as previously described [7]. Briefly, the cells were lysed in RIPA buffer (50 mM Tris-HCl, pH 7.5, 150mM NaCl, 1% NP-40, 0.5%

sodium deoxycholate, 0.1% SDS) and protease cocktail inhibitor I (Calbiochem, San Diego, CA). The cell lysates were separated on SDS-PAGE (10% or 12.5% polyacrylamide, EpiZyme, Shanghai) and transferred to polyvinylidene difluoride membranes (PVDF, Roche). The blots were blocked in TBST containing 5% skimmed milk and incubated with primary antibodies overnight at 4˚C. The membranes were washed with TBST 4×10 minutes and then incubated with secondary antibodies (Beyotime, Shanghai, China) for 1 h at room temperature. After three additional washes with TBST, immunoreactive bands were detected using enhanced chemiluminescence (Tanon, Shanghai, China), followed by exposure on ChemiDoc Touch Imaging System (BIO-RAD, Hercules, CA). The antibodies were listed as follows: CD8A (Abcam, ab237710, 1:1500); α-SMA (Sigma, Cat: A2547, 1:1000); (Gal1, NSJ bioreagents, Cat: R31653, 1:1000)

Immunofluorescence co-staining of CD8A and TUNEL in murine tumors.

Following excision from mice, tumor tissues were washed by PBS and fixed in 4 % paraformaldehyde overnight at room temperature, then embedded in the paraffin by standard procedures. Tissue blocks were sectioned at 4-μm thickness on a microtome, placed onto positively charged glass slides, and stained with H&E according to standard protocols. For immunofluorescence co-staining of CD8A, PANO 4-plex IHC kit (Panovue, 0079100020) was used. CD8A (Abcam, ab217344, 1:800) primary antibodies was incubated overnight at 4˚C, followed by horseradish peroxidase-conjugated secondary antibodies incubation and tyramide signal amplification. The slides were microwave heat-treated after tyramide signal amplification operation. Nuclei were stained with 4-6-diamidino-2-phenylindole (DAPI). Then incubated with TUNEL (Beyotime, C1086) for an hour at 37 ˚C. Images were captured by a confocal laser microscope (OLYMPUS FV1000, Tokyo, Japan), and counts of $CD8^+$ T cells and apoptotic $CD8^+$ T cells were calculated by HALO software (Indicalab, New Mexico, USA).

Mice and cell lines

Female BALB/c mice were purchased from Vital River (Beijing, China) and were maintained in specific pathogen-free conditions in the animal laboratory of SYSUCC. The murine cell line of renal cancer (Renca) was kindly provided by Professor Luo (Center for Precision Medicine, Sun Yat-sen University, Guangzhou, China), and the murine fibroblast line (NIH/3T3) was purchased from the National Collection of Authenticated Cell Cultures of China. Renal cancer-associated fibroblasts were isolated from human primary clear cell renal carcinoma as described previously.

Establishment of stable Gal1 knocking fibroblasts

Lentiviral vectors containing luciferase, Gal1 small hairpin (sh) RNA plasmid were purchased from Genechem Co., LTD (Shanghai, China) and prepared in accordance with standard protocols. Briefly, 3×10^6 293T cells were seeded in a 10 cm dish. After 24 hours incubation, cells were transfected with shRNA or negative control plasmids by Lipofectamine 3000 (Invitrogen). We changed the medium to remove transfection reagents after 8 hours and virus was collected 36 hours later. NIH/3T3 cells and human CAFs were transduced with sh-Gal1 or sh-NC lentiviruses for 24 hours. After 48 hours of lentivirus infection, cells were screened using puromycin (1 microg/ml) for 7 days to establish stably transduced cell lines. Cell lysates were prepared for protein extraction and then cell line with lower Gal1 protein expression was chosen (based on the Western blotting results) for further experiments.The shRNA target sequences for murine Gal1were: sh1: GTGTGTAACACCAAGGAAGAT and sh2:AGACGGACATGAATTCAAGTT. And The shRNA target sequences for human Gal1in were: sh1: GCCCACGGCGACGCCAACACC and sh2: GCTGCCAGATGGATACGAATT.

Isolation of human $CD8^+$ T cells

Peripheral blood mononuclear cells (PBMC) from health donor were first isolated from buffy coat by density gradient centrifugation using Lymphocyte Separation Medium (Biosharp). $CD8^+$ T cells were then isolated from PBMC using CD8

microbeads (Miltenyi Biotec), and purity was assessed by flow cytometry. Subsequent experiments were carried out after confirming $CD8^+$ T cell population was >95% pure. For all the experiments, $CD8^+$ T cells were cultivated with X-VIVO medium (LONZA) supplemented with 10% fetal bovine serum (FBS) at the density of 1.5×10^6 cells per ml per cm^2 with additional interleukin-2 supplement (100 IU/mL, Miltenyi Biotec.) and ImmunoCult™ Human CD3/CD28 T Cell Activator (10µl/mL, InvivoGen).

CAFs and $CD8^+$ T cells coculture system and flow cytometry analysis

It was reported that stromal cell in extracellular matrix is able to directly kill susceptible T cells via Gal1[10]. To investigate whether CAFs could induce $CD8^+$ T cells apoptosis and its potential regulators. We designed CAFs and CD8+ T cells coculture system according to previous study[10]. 5×10^5 CAFs in 2 ml of media were plated directly on solidified Matrigel (400 µl) in 6-well plates for 24 h, 3×10^6 $CD8^+$ T cells were added to Matrigel solidified and allowed to bind the Matrigel for 6 h. Media with unbound cells was aspirated and collected for analysis, Matrigel was digested by incubation in 800 µl of dispase (Invitrogen) for 40 min at 37°C. Digested cells incubated in 1 ml 2.5% Trypsin for 2 min at 37°C, and passed over a 40-µm filter. Digested cells and unbound cells were washed twice with PBS. $CD8^+$ T cells were then isolated using CD8 microbeads (Miltenyi Biotec) and then incubated with FITC Annexin V and PI at room temperature in the dark for 15 minutes. $CD8^+$ T cells apoptosis was assessed by flow cytometry.

***In vivo* experiments**

To evaluate CAFs decreased the infiltrated $CD8^+$ T cells in the tumor via expressing Gal1, we used 4 - 6 weeks old female BALB/c mice. Mice were anesthetized and 100µL of a single-cell suspension containing either Renca-luc (1×10^6 cells) with NIH/3T3 (Gal1-shNC) fibroblasts (1×10^6 cells), or Renca-luc (1×10^6 cells) with NIH/3T3 (shGal1) fibroblasts (1×10^6 cells) was injected into the right kidney cortex,

the renal orthotopic tumor were detected by luciferin (VivoGlo Luciferin, In Vivo Grade). Mice were sacrificed after 4 weeks by cervical dislocation under anesthesia, and tumors were harvested, and tumor volume were examined.

To analyze whether Gal1 expressed in CAFs could hamper the efficacy of immunotherapy *in vivo*, Renca (1×10^6 cells) with NIH/3T3 (shNC) fibroblasts (1×10^6 cells), or Renca (1×10^6 cells) with NIH/3T3 (shGal1) fibroblasts (1×10^6 cells) resuspended in 100 µl PBS were injected into the skin of the right flank of 4–6 weeks old male BALB/c mice[11]. Tumor growth was monitored every 3 days by measuring the length and width of the tumor. After tumors reaching approximately 50 mm^3, anti-PD1 (clone RMP1-14, BioXCell) was injected i.p. (200µg/mouse) every 2 days[12].

To investigate the Gal1 inhibitor OTX008 could increase the efficacy of immunotherapy, BALB/c mice were injected subcutaneously in the right flank with Renca (1×10^6 cells) and NIH/3T3 (shNC) fibroblasts (1×10^6 cells), when tumors reached 50 mm^3, mice were randomly assigned to 4 groups, namely control (vehicle), OTX008 (Selleck, 10mg/kg/mouse/2 days, administered intraperitoneally)[13], anti-PD1 (200µg/mouse /2 days, administered intraperitoneally) and OTX008 + anti-PD1.

The tumor volume was calculated using the formula: $0.52 \times \text{Length} \times \text{Width}^2$.

Statistical analysis

The data were analyzed using GraphPad Prism software version 8 (GraphPad Software, San Diego, California, US). Comparisons between paired pRCC and reRCC were performed with the paired Wilcoxon test. Others were performed with unpaired Wilcoxon test. We constructed survival curves using the Kaplan-Meier method, and their equality was compared via log-rank test. The tumor growth in mice was measured using the method of a repeated-measures ANOVA. All data are presented as means ± standard deviations (SDs). * $p < 0.05$, ** $p < 0.01$, *** $p < 0.001$. Statistical significance was set at p values less than 0·05.

Study approval

This study was performed in accordance with the ethical standards of the Helsinki Declaration and the ethical guidelines for Medical and Health Research Involving Human Subjects[14]. Written informed consent was obtained for each of the participant patients. All cases were de-identified and personal identifiable details were removed from their case descriptions to ensure anonymity. This study was approved and reviewed by the Ethics Review Board of Sun Yat-sen University Cancer Center. Mouse experiments were performed in a specific pathogen-free environment at the animal laboratory of the SYSUCC according to institutional guidelines, and all animal experimental protocols were approved and reviewed by the Ethics Review Committee for Animal Experimentation of SYSUCC. All experiments were performed in accordance with the guidelines and regulations indicated by these committees.

Refrence

[1] Young MD, Mitchell TJ, Vieira Braga FA, Tran MGB, Stewart BJ, Ferdinand JR, Collord G, Botting RA, Popescu DM, Loudon KW, Vento-Tormo R, Stephenson E, Cagan A, Farndon SJ, Del Castillo Velasco-Herrera M, Guzzo C, Richoz N, Mamanova L, Aho T, Armitage JN, Riddick ACP, Mushtaq I, Farrell S, Rampling D, Nicholson J, Filby A, Burge J, Lisgo S, Maxwell PH, Lindsay S, Warren AY, Stewart GD, Sebire N, Coleman N, Haniffa M, Teichmann SA, Clatworthy M and Behjati S. Single-cell transcriptomes from human kidneys reveal the cellular identity of renal tumors. Science 2018; 361: 594-599.

[2] Racle J, de Jonge K, Baumgaertner P, Speiser DE and Gfeller D. Simultaneous enumeration of cancer and immune cell types from bulk tumor gene expression data. Elife 2017; 6:

[3] Stuart T, Butler A, Hoffman P, Hafemeister C, Papalexi E, Mauck WM, 3rd, Hao Y, Stoeckius M, Smibert P and Satija R. Comprehensive Integration of Single-Cell Data. Cell 2019; 177: 1888-1902 e1821.

[4] Zhang M, Yang H, Wan L, Wang Z, Wang H, Ge C, Liu Y, Hao Y, Zhang D, Shi G, Gong Y, Ni Y, Wang C, Zhang Y, Xi J, Wang S, Shi L, Zhang L, Yue W, Pei X, Liu B and Yan X. Single-cell transcriptomic architecture and intercellular crosstalk of human intrahepatic cholangiocarcinoma. J Hepatol 2020; 73: 1118-1130.

[5] McGinnis CS, Murrow LM and Gartner ZJ. DoubletFinder: Doublet Detection in Single-Cell RNA Sequencing Data Using Artificial Nearest Neighbors. Cell Syst 2019; 8: 329-337 e324.

[6] Korsunsky I, Millard N, Fan J, Slowikowski K, Zhang F, Wei K, Baglaenko Y, Brenner M, Loh PR and Raychaudhuri S. Fast, sensitive and accurate integration of single-cell data with Harmony. Nat Methods 2019; 16: 1289-1296.

[7] Tirosh I, Izar B, Prakadan SM, Wadsworth MH, 2nd, Treacy D, Trombetta JJ, Rotem A, Rodman C, Lian C, Murphy G, Fallahi-Sichani M, Dutton-Regester K, Lin JR, Cohen O, Shah P, Lu D, Genshaft AS, Hughes TK, Ziegler CG, Kazer SW, Gaillard A, Kolb KE, Villani AC, Johannessen CM, Andreev AY, Van Allen EM, Bertagnolli M, Sorger PK, Sullivan RJ, Flaherty KT, Frederick DT, Jane-Valbuena J, Yoon CH, Rozenblatt-Rosen O, Shalek AK, Regev A and Garraway LA. Dissecting the multicellular ecosystem of metastatic melanoma by single-cell RNA-seq. Science 2016; 352: 189-196.

[8] Patel AP, Tirosh I, Trombetta JJ, Shalek AK, Gillespie SM, Wakimoto H, Cahill DP, Nahed BV, Curry WT, Martuza RL, Louis DN, Rozenblatt-Rosen O, Suva ML, Regev A and Bernstein BE. Single-cell RNA-seq highlights intratumoral heterogeneity in primary glioblastoma. Science 2014; 344: 1396-1401.

[9] Qiu X, Mao Q, Tang Y, Wang L, Chawla R, Pliner HA and Trapnell C. Reversed graph embedding resolves complex single-cell trajectories. Nat Methods 2017; 14: 979-982.

[10] He J and Baum LG. Presentation of galectin-1 by extracellular matrix triggers T cell death. J Biol Chem 2004; 279: 4705-4712.

[11] Kato T, Noma K, Ohara T, Kashima H, Katsura Y, Sato H, Komoto S, Katsube R, Ninomiya T, Tazawa H, Shirakawa Y and Fujiwara T. Cancer-Associated Fibroblasts Affect Intratumoral CD8(+) and FoxP3(+) T Cells Via IL6 in the Tumor Microenvironment. Clin Cancer Res 2018; 24: 4820-4833.

[12] Moynihan KD, Opel CF, Szeto GL, Tzeng A, Zhu EF, Engreitz JM, Williams RT, Rakhra K, Zhang MH, Rothschilds AM, Kumari S, Kelly RL, Kwan BH, Abraham W, Hu K, Mehta NK, Kauke MJ, Suh H, Cochran JR, Lauffenburger DA, Wittrup KD and Irvine DJ. Eradication of large established tumors in mice by combination immunotherapy that engages innate and adaptive immune responses. Nat Med 2016; 22: 1402-1410.

[13] Koonce NA, Griffin RJ and Dings RPM. Galectin-1 Inhibitor OTX008 Induces Tumor Vessel Normalization and Tumor Growth Inhibition in Human Head and Neck Squamous Cell Carcinoma Models. Int J Mol Sci 2017; 18:

[14] Ogasawara K. [8. Revised "Ethical Guidelines for Medical and Health Research Involving Human Subjects"].

Supplementary Figures and figure legends.

Figure S1

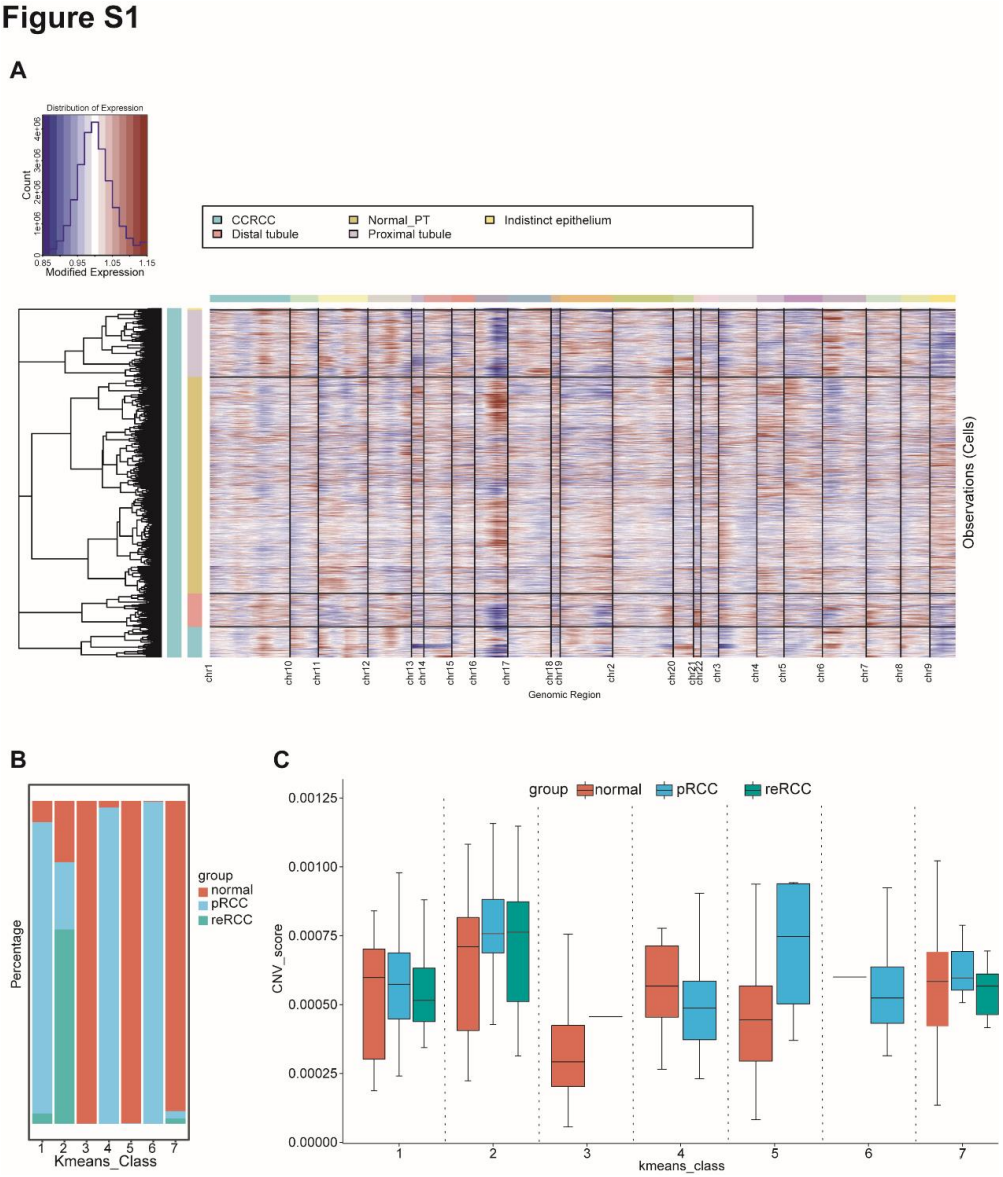

Figure S1 Detecting malignant cells using CNV analysis and kmeans clustering.

A. CNV analysis of epithelial cells.

B. Histogram showing the percentage of cell in kmeans class by groups.

C. Box plots showing the CNV score for kmeans class in each group.

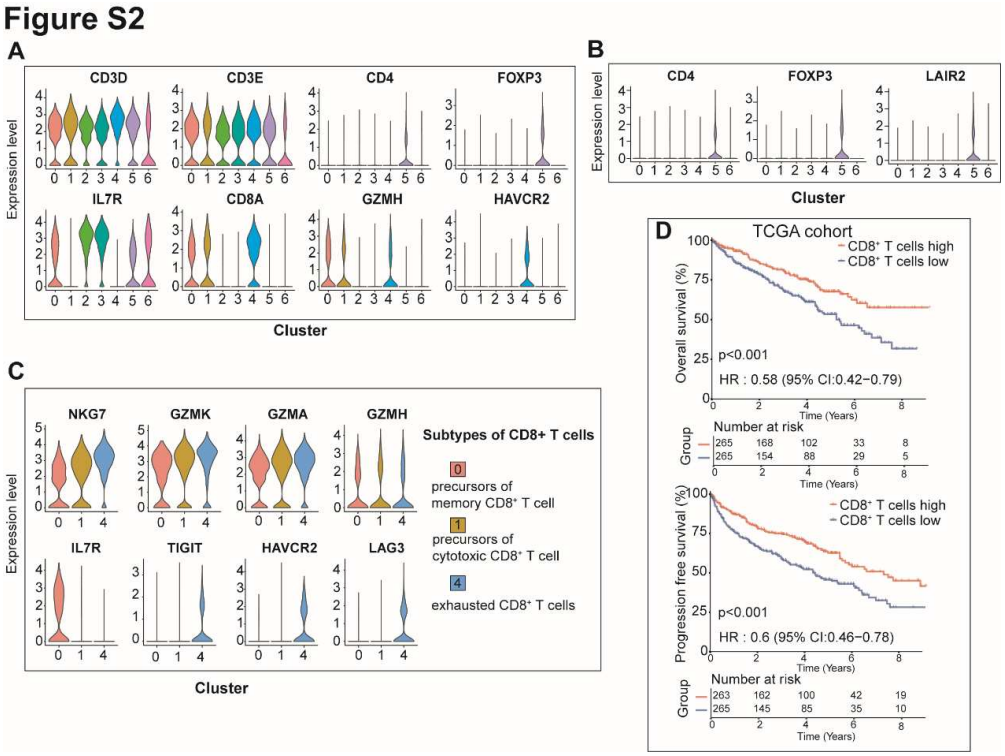

Figure S2

A. Violin plots showing the markers of subtypes of T cells.

B. Violin plots showing the markers of Tregs were specifically expressed in cluster5 of T cells.

C. Violin plots showing the genes of cytotoxicity were specifically expressed in $CD8^+$ T cells, and marker genes of 3 subtypes of $CD8^+$ T cells.

D. K-M curves showed a high infiltrating level of $CD8^+$T cells was significantly associated with longer overall survival and progression-free survival in RCC patients in the TCGA cohort.

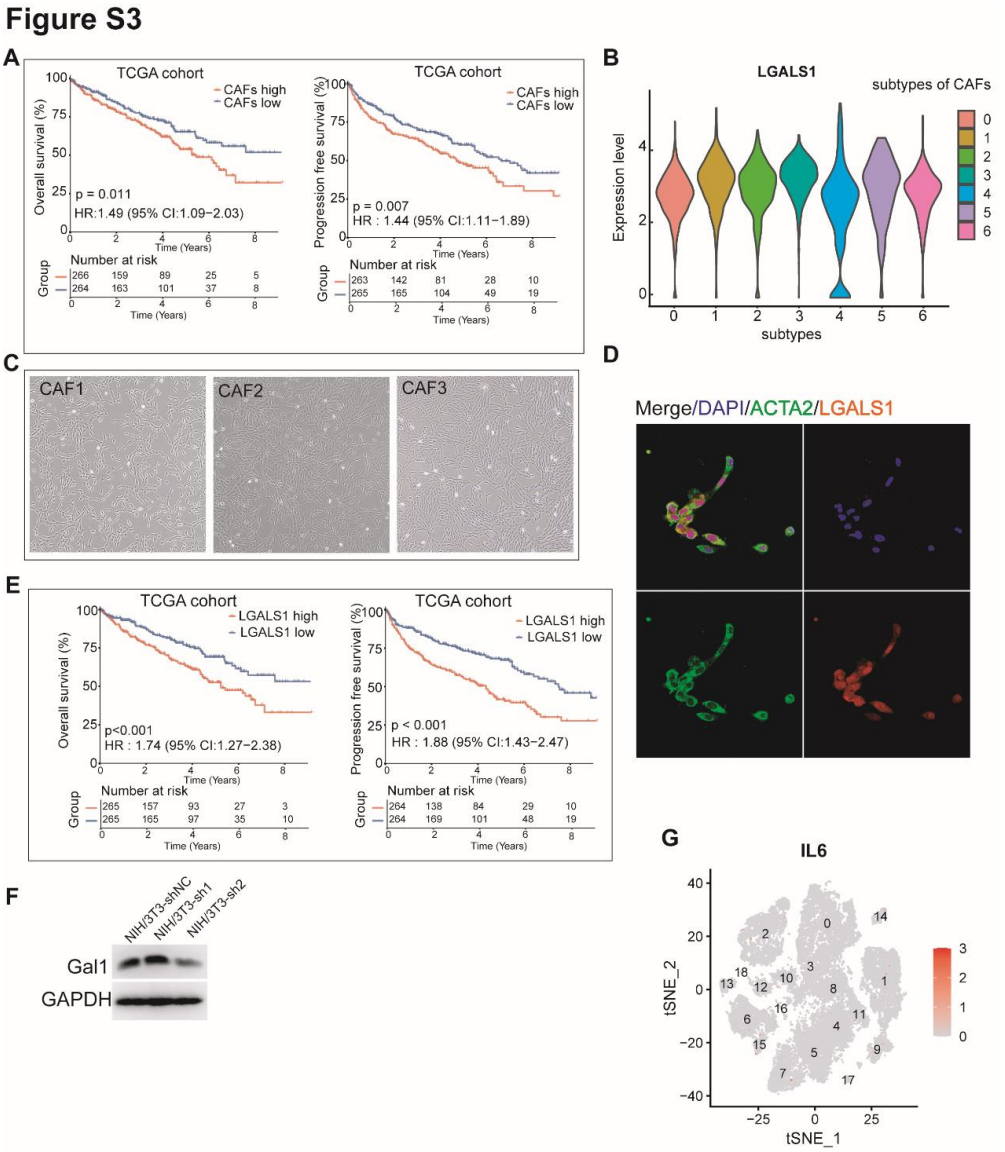

Figure S3

A. K-M curves showed a high infiltrating level of CAFs was significantly associated with poorer overall survival and progression-free survival in RCC patients in the TCGA cohort.

B. LGALS1 expressed high in 7 subclusters of CAFs.

C. Isolating and culturing primary CAFs from RCC patients

D. Multiplexed immunofluorescent staining of α-SMA and Gal-1 in primary CAFs.

E. K-M curves showed a high expression level of Gal-1 was significantly associated with poorer overall survival and progression-free survival in RCC patients in the

TCGA cohort.

F. Establishing and validating knocking down Gal1 in NIH/3T3 cell lines.

G. tSNE plot showing IL6 expressed extremely low in all cell types in RCC.